Cerebral hemodynamics: a mathematical model including autoregulation, baroreflex and extracranial peripheral circulation

Francisco Ambrosio Garcia[1*], Deusdedit Lineu Spavieri Junior[1¤], Andreas Linninger[2]

1 Division of Data Science, brain4care, São Carlos, State of São Paulo, Brazil.
2 Laboratory for Product and Process Design (LPPD), Department of Bioengineering and Chemical Engineering, University of Illinois at Chicago, Chicago, Illinois, United States of America.

* franc.ambr10@gmail.com ¤dspavieri@gmail.com

Abstract

Increasing evidence supports that cerebral autoregulation and mean arterial pressure regulation via baroreflex contribute to cerebral blood flow regulation. It is unclear whether the extracranial vascular bed of the head and neck helps reestablishing cerebral blood flow during changes in mean arterial pressure. Current computational models of cerebral blood flow regulation do not address the relationships between the intracranial and extracranial blood flow dynamics. We present a model of cerebral autoregulation, extracranial peripheral circulation and baroreflex control of heart rate and of peripheral vasculature that was included to the model of intracranial dynamics proposed by Linninger et al. (2009), which incorporates the fully coupled blood, cerebrospinal fluid and brain parenchyma systems. Autoregulation was modelled as being pressure-mediated at the arteries and arterioles and flow-mediated at the microcirculation. During simulations of a bout of acute hypotension, cerebral blood flow returns rapidly to baseline levels with a very small overshoot, whereas the blood flow to the peripheral circulation of the head and neck suffers a prolonged suppression in accordance with experimental evidence. The inclusion of baroreflex regulation at the extracranial vascular bed had a negligible effect on cerebral blood flow regulation during dynamic changes in mean arterial pressure. Moreover, the results suggest that the extracranial blood flow carries only modest information about cerebral blood flow in dynamic situations in which cerebral autoregulation is preserved and mean arterial pressure suffers alterations. This information is likely higher when the autoregulation is impaired. Steady-state cerebral blood flow in the model is kept within normal ranges despite variations in mean arterial pressure from 50 to 175 mmHg. By inputting aortic pressure waves from individuals with increasing arterial rigidity, increasing arterial systolic and pulse pressures, the model predicts the generation of intracranial pressure waves with accordingly increasing peaks and amplitudes.

Introduction and Motivations

Cerebral autoregulation (CA) is believed to comprise a multitude of cerebrovascular and neurogenic mechanisms that keep the cerebral blood flow (CBF) in normal ranges despite variations in the cerebral perfusion pressure (CPP) from 50 to 150 mmHg [1]. In addition to the local CA, there is increasing evidence that the systemic blood pressure

regulation via baroreflex plays a role in maintaining CBF [2–4]. Baroreflex acts for example on the total peripheral resistance by modulating sympathetic nerve activity. However, the sympathetic effect on the extracranial vascular bed and the relations between the intracranial and extracranial circulations are not completely understood [4]. A better understanding of the intracranial and extracranial hemodynamics may improve the assessment of the intracranial state by non-invasive, yet superficial tissue dependent, extracranial measurements such as functional Near-Infrared Spectroscopy [5–7] and noninvasive intracranial pressure (ICP) monitoring by strain gauge [8]. The existence of relations between intracranial and extracranial circulations could even allow the assessment of the intracranial state by measurements only on the external blood flow.

The authors in [3, 4] recorded the blood flow at the internal (ICA) and external carotid (ECA) arteries during a bout of acute hypotension caused by thigh-cuff inflation-deflation. The ICA blood flow dropped (26.7% in [3], 16.8% in [4]-control) and returned rapidly to baseline levels thanks to CA and baroreflex, showing an overshoot (23.8% in [3], 8.1% in [4]-control) followed by an oscillatory behavior in [3]. This rapid return to baseline levels followed by oscillations was also found in the middle cerebral artery mean blood velocity [3] and in the blood flow on the posterior cerebral artery after a squat-stand maneuver, which induces an acute drop in blood pressure [9]. The ECA blood flow, on the contrary, dropped (42.0% in [3], 41.2% in [4]-control) and remained below baseline levels for a prolonged time returning gradually according to a damped dynamic in [3, 4].

The prolonged recovery time in the ECA blood flow initially indicated that the vascular bed of the head and neck constrict due to an increase in sympathetic tone via baroreflex, contributing to the reestablishment of CBF [3]. Previously, [10] proposed that the difference between the blood flow in the ICA and in the ECA during induced hypovolemic hypotension in monkeys is caused by heterogeneous sympathetic innervation of the ECA and the ICA vascular beds.

However, more recent work suggests that the vascular bed of the ECA is not regulated by sympathetic activity and does not contribute to CBF regulation during acute hypotension in healthy young men [4]. Previous experiments similarly suggested that the extracranial vasculature is passive [11].

A computational model of intracranial dynamics that accounts for regulatory mechanisms and the extracranial vascular bed may help elucidate the relations between intracranial and extracranial dynamics. Many models have already been proposed to explain mechanisms underlying experimental evidence, such as the compensatory role of the Circle of Willis during internal carotid occlusion [12]. However, the role of the extracranial vasculature on CBF regulation has not yet been addressed in computational models.

Moreover, understanding how CBF is affected by episodes of hypotension, both in healthy and impaired conditions is important. Dynamic tests such as thigh cuff inflation-deflation may help monitoring the regulatory capacity in head injury patients [13], although they are not considered to be the preferred methods [14]. Additionally, it is known that regulatory mechanisms of CBF become impaired in patients with traumatic brain injury. During treatment, these patients often suffer from episodes of hypotension caused by hypnotic drugs or secondary injuries, which can lead to ischemic brain damage [15]. For instance, propofol, which is a commonly used drug in intensive care units, caused a reduction of 20.4% and 10.6% in the systolic and diastolic pressures, respectively, within 4 min after the intravenous injection in [16]. The results in [16] suggested that the propofol-induced hypotension is likely caused by inhibition of the sympathetic nervous system and impairment of baroreflex.

Finally, we remark our interest on the effects of an aging vascular system on the ICP wave. Usually the arterial pulse pressure increases and the arterial reflected wave arrives

earlier in individuals with increased arterial rigidity, causing a change in the arterial waveform marked by an augmented P2/P1 ratio [17–19]. Previous work [20] hypothesized that the ICP wave is governed by the change in cerebral blood volume at each cardiac cycle and by the cerebrospinal elastance. In this manner it is relevant to investigate how changes in the arterial pressure wave affect the ICP wave.

Therefore we develop a model of intracranial dynamics that includes CA, baroreflex and peripheral extracranial circulation based on the previous model proposed by Linninger et al. (2009) [21]. In the next section we will briefly describe the mechanisms of cerebral autoregulation and the baroreflex system, which will be simplified and added to the model later on.

Background

Cerebral autoregulation

CA includes four mechanisms: myogenic, metabolic, endothelial and neurogenic [1, 22].

Myogenic mechanism. The smooth muscle of small cerebral arteries and arterioles contracts when the intralumial pressure increases and relaxes when the pressure decreases [1, 23]. This mechanism has the fastest dynamics. In rats cerebral and mesenteric small arteries it started to act with a delay usually less than 250 ms in [24]. A median time constant in the order of 6.75 s fitted from eight subjects was found in [9]. Note that delay means a dead time during which the mechanisms have no action, while time constant indicates the time after the initial delay needed to achieve 63.2% of the final value in response to a step. This mechanism was included in the model as being pressure-mediated at the arteries and arterioles compartments.

Metabolic mechanism. Many pathways cause vasomotor changes in small vessels, such as terminal arterioles and capillaries, as a function of tissue metabolism [1, 9, 25–27]. For example, high P_{CO_2} and low tissue P_{O_2} cause significant relaxation of cerebral blood vessels [22]. Other contributing factors are tissue concentration of adenosine, lactate, and pH [22]. The time constant of the metabolic mechanism is in the order of 20 s [28]. This mechanism was included in the model as being flow-mediated at the microcirculation compartment.

Endothelial mechanism. Several factors influence the secretion of vasodilators and vasoconstrictors by endothelial cells of brain blood vessels. For example, the secretion of NO contains a shear stress response element [22]. The endothelial mechanism is usually modeled as being flow-mediated because shear stress is directly caused by viscous friction of blood and the wall of endothelial cells. It is a slower process with time constant of approximately 60 s [9]. This mechanism was neglected in the model due to its lower contribution when compared to the myogenic one [9].

Neurogenic mechanism. Neural activity affects the smooth muscle tone of small and medium-sized vessels because cells such as neurons, astrocytes and microglia release neurotransmitters with vasoactive properties [9, 26]. For example, neurons secrete NO during activation, which may contribute to increase blood flow [22]. The median time constant was found to be in the order of 8.5 s in [9]. This mechanism was not included in the model because it would require an additional input corresponding to the neural activity, which is beyond the goal of our paper

Table 1 summarizes the main aspects of the cerebral autoregulation mechanisms and shows whether or not they are included in our model.

Table 1. Overview of cerebral autoregulation mechanisms and their inclusion in the model

Mechanism	Main factors	Local of action	Time constant (s)	Model
Myogenic	Intralumial pressure [24]	Small arteries and arterioles [23]	1 [29] to 10 [9]	Arteries and arterioles
Metabolic	P_{CO_2}, P_{O_2} [22]	Small vessels [1]	20 [28]	Microcirculation
Endothelial	Shear-stress [9, 22]	Arteries and arterioles [9]	60 [9]	Not included
Neurogenic	Neural activity	Small and medium-sized vessels [26]	8.5 [9]	Not included

Baroreflex

The short-term mean arterial pressure (MAP) is controlled mainly by the baroreflex [30]. MAP regulation indirectly influences CBF (indirect regulation). Baroreflex also causes less clear direct vasomotor changes in cerebral blood vessels by modulating sympathetic and parasympathetic activities (direct regulation) [2].

MAP and its rate of change are sensed by baroreceptors, nerve endings that sense stretch, located at the carotid sinuses, especially along the medial wall of the ICA near the common carotid bifurcation [31], and at the aortic arch [32]. The MAP regulates the firing rate of the sensory neurons, which transmit the signals to central integrating centers primarily at the medulla oblongata [33] trough afferent pathways, affecting both sympathetic and parasympathetic tones [33, 34]. In addition to the aforementioned baroreceptors, recently it was shown in rats that astrocytes contribute to sympathetic activity, acting as baroreceptors in the brain sensing CPP [35].

Sympathetic tone modulates the peripheral resistance, venous capacitance mostly in the splanchnic region, HR and heart contractility [34]. The effects of sympathetic activity on different variables are modeled with time constants varying from 3 to 30 s depending on the effector organ [36, 37]. [38] considered a pure delay of 7 s.

Parasympathetic tone modulates heart rate (HR), modeled with time constants of 3 to 4 s [36, 37], usually without any additional pure delay.

Indirect regulation. It corresponds to the indirect contribution of MAP regulation to maintaining CBF [2]. Fig 1 presents the indirect effect of MAP regulation via baroreflex on CBF when MAP drops. We included in the model the control of peripheral vasculature and HR control. The closed-loop mean arterial pressure regulation was not modeled since the pressure at the base of the common carotid artery is the input to our model.

Direct regulation. The direct effect corresponds to alterations in the cerebral vasculature due to the baroreflex and is less clear [41]. In normal conditions, the existing literature reports limited effect in humans, even tough cerebral vessels are innervated with sympathetic nerve fibers [2]. In dynamic situations, [4] discusses that sympathetic activity likely plays a role in regulating cerebral vasculature and might regulate ICA vasoconstriction during acute hypotension. In rats it was demonstrated that parasympathetic activity influences cerebrovascular tone [42], especially during acute hypertension [43]. We did not include direct effects of baroreflex on the brain vessels.

We briefly discussed the mechanisms of cerebral blood flow regulation. In the following we will present the mathematical models that have been proposed to describe such systems.

Mathematical models

Mathematical models are useful tools to study brain hemodynamics, helping to explain evidence from clinical trials [44]. The model's accuracy depends on the degree of detail [45], simulation time scale, availability of real data to build the model, patient specificity, etc [44].

Fig 1. MAP regulation via baroreflex and its indirect effect on CBF. When MAP decreases, CBF also decreases. Baroreflex regulation of MAP induces an increase in HR, increase in total peripheral resistance (PR), increase in cardiac contractility and decrease in venous capacitance. These variables affect the stroke volume (SV). In steady-state conditions, an increase in HR is associated to a decrease in SV [39]. Cardiac output (CO) is the product of HR and SV [40]. In steady-state the increase in HR outperforms the decrease in SV, so CO ends up increasing [39]. In specific dynamic situations such as after an acute bout of hypotension caused by a thigh-cuff release, it is thought that SV remains transiently constant, so the increase in CO is proportional to the increase in HR [2]. In both cases MAP increases because it is the product of CO and total peripheral vascular resistance [33], which closes the negative feedback loop. This helps reestablishing CPP, and consequently, CBF, which is also influenced by CO [4].

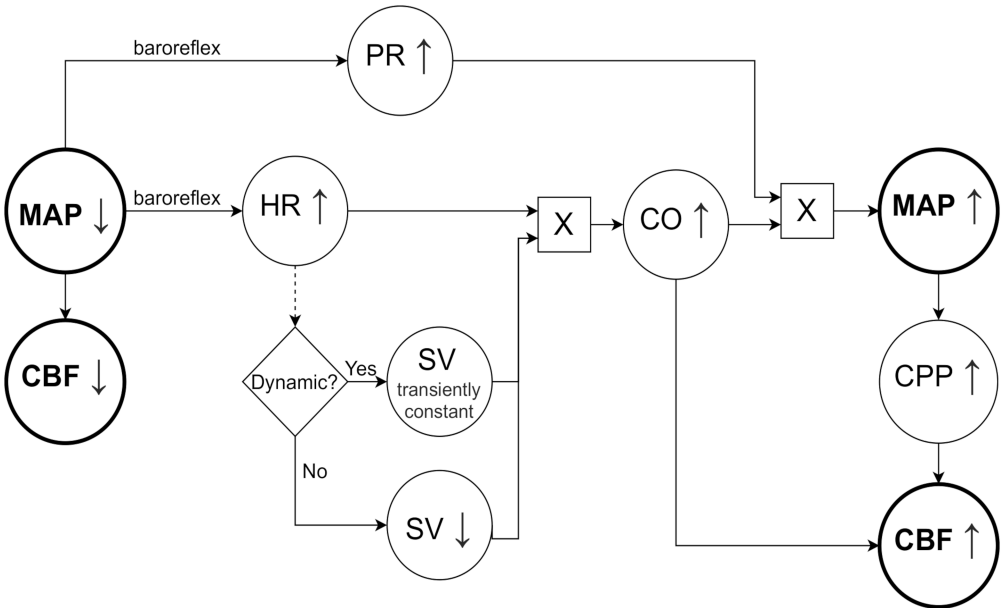

Several models of CBF regulation exist. The first models [46, 47], which were later simplified to [48], included a single ICP compartment and a single pressure or flow-mediated regulatory mechanism in an attempt to mimic the aggregated behavior of the CBF regulation. [28] included a pressure-mediated, a flow-mediated mechanism and their nonlinear interaction with CO_2 reactivity. The model distinguished the different gains and time constants found in large and small pial vessels. Later, [12] increased the degree of detail of the cerebral vasculature, most notably to include the circle of Willis. Each active compartment was self-regulated.

The Linninger model [21] offers a more detailed description of the CSF system and includes the bilateral brain parenchyma, but the original work did not address blood flow regulation. [49] expanded the cerebral circulation model in [50] to include two autoregulation mechanisms, but the CSF system was not addressed. [9] included four autoregulation mechanisms acting on a single arteriolar compartment and the ICP was considered constant. Other approaches include neural networks and transfer functions [51]. For a more complete review of the autoregulation models, we refer the reader to [52].

Many researchers have also attempted to model the complex regulation of MAP trough baroreflex, from focusing on a single aspect of the system, such as the heart rate [38, 53], to the complete system [36]. [37] analysed the short-term MAP regulation in response to a head up tilt test. Although physiological systems are continuous, some

models may assume that the controlled variables remain constant within a heartbeat, for example using a discrete-time coupled system of equations [54].

A few models included both CA and baroreflex mechanisms. [55] and [56] have shown to be the models in the literature closest to our goal here in this paper. [55] included the MAP regulation via baroreflex in closed loop and CA only at the arteries. Although the model contains capacitances of the arteries and veins of the neck, their contribution to CBF was not addressed. The compliance of the intracranial space was lumped to a single capacitance.

[56] included more than one element on the cerebrospinal fluid (CSF) system but the overall compliance of CSF space was lumped to a single capacitance. They included the myogenic and CO_2 reactivity mechanisms on a single side of the brain to study the impact of the regulatory asymmetry.

Tables 2 and 3 present our literature review on models of intracranial dynamics, baroreflex and CBF regulation. Baroreflex models of a single aspect were excluded.

Here we aim to develop a model of the intracranial dynamics that includes simple cerebral autoregulation mechanisms that capture the main factors as function of the sizes of the vessels, baroreflex control of HR and of peripheral vasculature and the peripheral circulation of the head and neck, which may act as a vascular bed to CBF. Moreover, our model is intended to be able to simulate pulsatile ICP, incorporating the main compartments of the CSF system and the brain parenchyma.

Materials and methods

Ethics Statement

In this study no experiment in humans nor in animals was performed, therefore no approval from an Institutional Review Board nor from an ethics board for animal research was required. Since this study did not involve any participant, participant consent is not applicable. No medical records nor archived samples were accessed.

Overview of the model of intracranial and peripheral blood circulation, cerebrospinal fluid, brain parenchyma, cerebral autoregulation and baroreflex

In the following sections we give an overview of all the systems included in our model, then we briefly review the seminal model [21] and finally we describe the addition of cerebral autoregulation, baroreflex and the expansion of the arterial network.

A model of the intracranial cerebral vasculature divided into compartments representing left and right [arteries, arterioles, microcirculation, veins] and venous sinus which is common to both sides was derived from the Linninger model [21]. The Linninger model [21] was chosen because it integrated results from extensive magnetic resonance imaging studies [65–68] with detailed two and three-dimensional mathematical models. These insights were condensed into a comprehensive mathematical description of the major intracranial dynamics with fluid structure interactions of blood, cerebrospinal fluid in the ventricular system, as well as cranial and the spinal subarachnoid spaces and the deformable brain parenchyma. It includes the ventricular CSF system divided into left and right lateral ventricles (Lvs), third (3V) and fourth ventricles (4V), cerebral subarachnoid space (cSAS) and spinal canal. Lvs are connected to the 3V, which is connected to the 4V. 4V communicates with the cSAS which is connected to the spinal canal. The brain parenchyma is modeled as an incompressible solid cell matrix surrounded by extracellular fluid and is split into right and left hemispheres.

Table 2. Overview of intracranial dynamics, baroreflex and cerebral autoregulation models - part 1.

Ref	Focus of study	CSF and brain parenchyma systems	PL ICP?	Cerebral autoregulation	BaR	EC
[46, 47]	Genesis of the intracranial pressure wave, blood flow in cerebral basal arteries, saline injections and obstruction in the cerebral venous return.	Single capacitance	Yes	Single pressure-mediated	None	Extracranial veins
[57]	Arterial hypotension, generation of plateau waves.	Single capacitance	Yes	Pressure-mediated at large vessels, flow-mediated at small vessels	None	Extracranial veins
[48]	Generation of plateau waves, acute hypotension, pressure-volume index tests.	Single capacitance	No	Single flow-mediated	None	None
[28]	Nonlinear interaction of CO_2 reactivity with autoregulation.	Single capacitance	No	Pressure-mediated at large pial arteries, flow-mediated at small pial arteries and their nonlinear interaction with CO_2 reactivity	None	Extracranial veins
[12]	ICA compression tests, stenosis of ICA and MCA and the role of the Circle of Willis.	Single capacitance	Yes	Pressure-mediated at large pial arteries, flow-mediated at small pial arteries and their nonlinear interaction with CO_2 reactivity	None	ICAs, basilar artery
[58]	Relations between cerebrovascular dynamics, ICP, Cushing response and short-term MAP regulation.	Single capacitance	Yes	Flow-mediated and nonlinear interaction with CO_2 reactivity	Complete system	Extracranial veins
[59]	Simulated MAP and MCA blood flow velocity during postural change from sitting to standing.	Brain resistance	No	Empirical model based on piecewise linear functions	Partial	None
[55]	Interactions between cerebral autoregulation and brain gas exchange during carotid artery compression, short/long-term arterial hypotension.	Single intracranial compliance, interstitial and intracellular spaces have constant volumes	Yes	Flow-mediated at arteries and effect of CO_2	Complete system	Neck arteries and veins
[21]	Predicted intracranial pressure gradients, blood and CSF flows in normal and in communicating hydrocephalus conditions.	Biphasic brain parenchyma, lateral, third and fourth ventricles, cSAS, spinal cord	Yes	None	None	Jugular veins are boundary condition
[56]	Studied the effect of regulatory asymmetry on blood flow and predicted the interhemispheric steal effect.	Single capacitance, left and right cSASs and cerebral aqueduct are resistances	Yes	Pressure-mediated and CO_2-mediated acting on single element	None	ICAs and venous outflow compliances

Ref: Reference. PL: Pulsatile. ICP: intracranial pressure. BaR: baroreflex. EC: Extracranial circulation. ICA: Internal carotid artery. MCA: Middle cerebral artery. MAP: Mean arterial pressure. CSF: Cerebrospinal fluid. cSAS: Cranial subarachnoid space.

Table 3. Overview of intracranial dynamics, baroreflex and cerebral autoregulation models - part 2.

Ref	Focus of study	CSF and brain parenchyma systems	PL ICP?	Cerebral autoregulation	BaR	EC
[49]	Coupling previous model of cerebrovascular bed [50] with autoregulation models.	None	No	Tested empirical model based on polynomial functions, a simple model and an optimal control model	None	None
[37]	Simulated the short-term pressure regulation during the tilt test.	None	No	None	Complete system	3D model of left and right [subclavians, CCAs bifurcating into ICAs and ECAs]
[36]	Effect of baroreflex during hemorrhage in the abdominal aorta artery and on cerebral aneurism in the presence of a regurgitating aortic valve.	None	No	None	Complete system	All main arteries
[9]	Cerebral autoregulation and neurovascular coupling in response to squat-stand maneuvers and visual stimulation.	None	No	Myogenic, metabolic, endothelial, neurogenic	None	None
[60]	Contribution of myogenic, shear-stress based and metabolic mechanisms with a theoretical model.	None	No	Myogenic, metabolic, shear-stress based	None	None
[61]	Studied the impact of bilateral traverse sinus stenosis on cerebral venous flow and CSF dynamics, as well as treatment strategies.	Same as [21]	Yes	None	None	Detailed description of head and neck veins
[62]	Predicted subject-specific flows and pressures in the ventricular system and subarachnoid space.	Entire cSAS and ventricular system in 3D	Yes	None	None	None
[63]	Simulated orthostatic stress tests.	None	No	None	Complete system, including cardiopulmonary reflex	None
[64]	Studied the cardiovascular response to centrifugation and lower body ergometer exercise.	None	No	None	Complete system, including cardiopulmonary reflex	None

Ref: Reference. PL: Pulsatile. ICP: intracranial pressure. BaR: baroreflex. EC: Extracranial circulation. CCA: Common carotid artery. ICA: Internal carotid artery. ECA: External carotid artery. CSF: Cerebrospinal fluid. cSAS: Cranial subarachnoid space.

We expanded the arterial network of the Linninger model to include the bifurcation of the common carotid artery (CCA) into the ICA and ECA arteries to mimic the distribution of blood supply to the brain and to the peripheral circulation of the head

and neck. The compartment originally denoted by capillaries here is denoted as microcirculation to represent the terminal arterioles, the capillaries and the venules, taken from [69]. The venules in [21] were therefore removed.

Here, the blood flows from the the CCA tube that bifurcates into the ICA, which supplies the intracranial vessels, and the ECA tube, which supplies the extracranial [arteries, microcirculation and veins], representing the head and neck peripheral circulation. The ICA is divided into the extracranial (ExICA) and intracranial (IcrICA) segments. We also added simple local CA mechanisms acting on the intracranial [arteries, arterioles and microcirculation], and baroreflex control of HR and of peripheral vasculature. Fig 2 shows an overview of the physiological systems included in the model.

The Linninger model of intracranial dynamics

In this section the Linninger model [21] is briefly explained.

Cerebral blood flow

In [21] the brain is supplied by a single carotid compartment which bifurcates into right and left cerebral arteries, arterioles, capillaries, venules and veins which converge to the venous sinus. Finally the blood flows to the jugular veins which are a boundary condition consisting of a constant venous pressure (p_{out}).

CSF system

The CSF production occurs at the choroid plexuses which consist of capillaries and connective tissue separated from the ventricles by epithelial cells [71]. CSF production is modelled as a constant term of fluid exchange between the microcirculation and lateral ventricles. The model also accounts for fluid exchange between the brain extracellular fluid and the lateral ventricles.

After passing trough the third and fourth ventricles and the cranial subarachnoid space (cSAS), the CSF is reabsorbed by the venous sinus according to a reabsorption resistance. The cSAS is communicating to the spinal canal, which is free to expand, contrarily to the intracranial compartments whose total volume is maintained constant by enforcing the Monro-Kellie doctrine separately at each side of the skull.

Brain parenchyma

The brain parenchyma is modeled as a solid cell matrix with constant volume surrounded by a extracellular fluid compartment which may expand, and is split into right and left hemispheres. The extracellular fluid may seep from the capillary bed into the brain in both directions according to the pressure gradient and an exchange resistance. Here it is important to remark that the incompressible cell matrix is a strong assumption that cannot capture for example plastic deformations on the brain tissue [21].

Arterial expansion and inclusion of control mechanisms

We added or modified the following elements to the Linninger model:

Extracranial (ExICA) and intracranial (IcrICA) internal carotid compartments

Approximately 3/4 of the brain blood supply comes from the internal carotid arteries and 1/4 from the vertebral arteries [41]. Here the flow at the intracranial ICA

Fig 2. Physiologically-based representation of systems in the model. Overview of physiological systems, based on figures from references [1, 21, 33, 70]. Intracranial and peripheral circulation, CSF system (light blue), biphasic brain parenchyma, cerebral autoregulation and baroreflex mechanisms are included in the model. The model considers that intracranial vessels are supplied by the internal carotid artery (ICA), which is split into the extracranial (ExICA) and intracranial segments (IcrICA). The external carotid (ECA) supplies the extracranial [arteries (ExAr), microcirculation (Exμ_{circ}) and veins (ExV)]. CSF is produced at the choroid plexus and reabsorbed at the venous sinuses. There is fluid exchange between the brain extracellular fluid and the microcirculation. Brain extracellular fluid and the lateral ventricles may also exchange fluid in both directions. We included simple local cerebral autoregulation (CA) mechanisms that are pressure-induced at the arteries (Ar) and arterioles (Al) and flow-induced at the microcirculation (μ_{circ}), which will be explained later. In the model, the pressure at the ExICA is sensed by baroreceptors affecting both sympathetic and parasympathetic tones. The heart rate is controlled by parasympathetic and sympathetic activities. We simulated both the cases in which the peripheral vasculature of the head and neck (ECA + ExAr) is and is not controlled by sympathetic activity, since it is known that noradrenaline and phenylephrine infusion induce facial vasoconstriction, but the ECA vasculature may not be regulated by sympathetic tone [4]. The pressure at the base of the common carotid artery (CCA) is the input to the model (p_{init}), so the closed-loop control of the mean arterial pressure (MAP) via baroreflex was not modelled.

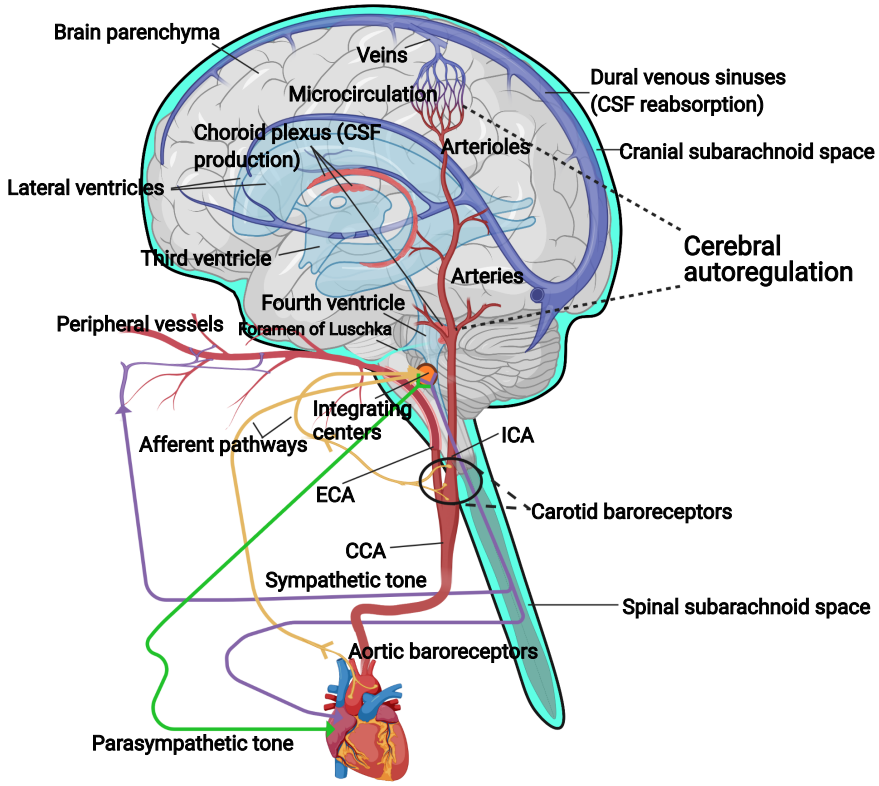

compartment is intended to mimic the total CBF.

The total ICA length is about 17.7 cm [72] whereas its extracranial part is about 8.6 cm [73]. We model the brain supply as two compartments in series: extracranial ICA

(ExICA) and intracranial ICA (IcrICA) segments with total volume of 5.19 cm^3 (V_0), which is equal to the total volume of the ICAs and vertebral arteries taken from [74]. We arbitrarily enforced the ExICA area at rest to be the double of the IcrICA area and the elastance to be the half.

Physiologically, the vertebral arteries, whose volume was included in the ICA tubes, branch from the subclavian arteries, not from the CCA. The IcrICA is included in the Monro-Kellie equations. These compartments substituted the original single carotid compartment.

External carotid (ECA), extracranial [arteries (ExAr), microcirculation (Exμ_{circ}), veins (ExV)] compartments

At baseline levels the average ICA blood flow is in the order of 1.5 times the ECA blood flow [3]. The head and neck receive about 4% of the cardiac debt, whereas the brain receives the triple, in the order of 12% of the cardiac debt [74]. Therefore we chose the total extracranial (ECA + ExAr + Exμ_{circ} + ExV) resistance to enforce a blood flow ratio between cerebral and peripheral circulation in the order of 3, instead of a blood flow ratio of 1.5.

Assuming a total blood volume of 4.9 l [75], the total volume at rest of the extracranial compartments was calculated to be 239.86 ml, because the head and neck contain about 4.895% of the total blood volume [74]. The ECA length of 6.10 cm was taken from [74], and the ECA area was $2\pi r_{ECA}^2$, where $r_{ECA} = 0.2265$ cm is the ECA internal radius [74]. The total length of the extracranial compartments of 20 cm was chosen arbitrarily.

Common carotid compartment (CCA)

The input to our model is the arterial blood pressure (ABP) at the base of the common carotid, which splits into the ICA and ECA arteries. Its length was taken as the average of the right and left common carotids lengths [74] and its area was $2\pi r_{CCA}^2$ where $r_{CCA} = 0.3029$ cm is the common carotid lumen radius [74].

Microcirculation

The Linninger model contains a compartment called Venules (Vl) and one called Capillaries (Cp). The volume of Cp in [21] was taken from the microcirculation tube in [69], which already includes the volume of the terminal arterioles, the capillaries and the venules. Therefore we decided to remove the Vl compartment and rename the Cp compartment to Microcirculation.

Autoregulation mechanisms

CA takes place most notably from the small cerebral arteries [1] up to small arterioles and capillaries [25]. The percentual changes in vessels diameters and their time constants are highly heterogeneous depending on the brain region and vessel sizes [76]. Instead of calculating the separate contribution of each autoregulation mechanism to each compartment, we developed a simpler model which is intended to grasp the main characteristics of CA in function of the vessels' sizes [77]. We therefore chose different input variables and parameters to each controlled compartment. Our autoregulation does not consider the neurogenic mechanism because we did not add an input to the model corresponding to the neural activity.

Usually the large cerebral arteries (ICA, middle and vertebral) are modeled as passive elements [9, 28]. Similarly, we assume that the ICA is not regulated. This assumption is supported by [78], which reported that the mean diameter of large

cerebral arteries changed less than 4% in patients during craniotomy under altered MAP and end tidal carbon dioxide, whereas smaller arterial diameters changed more than 20%. Despite this, the ICA vasculature may be regulated by sympathetic tone [4], but the evidence is limited.

For the intracranial arteries, arterioles and microcirculation, we consider that each compartment is self-regulated, which is in accordance with the local action of the myogenic and shear stress-based mechanisms. Physiologically this local action does not hold completely true. For example, the metabolic mechanism may act upstream with the diffusion of CO_2 from the microenvironment to arterioles [9].

The myogenic mechanism acts on small arteries and arterioles [23], and when compared only to the endothelial shear stress-based mechanism, it highly dominates both in short-time regulation and in steady state [9]. We assume in this manner that the input to the autoregulation of both the arterial and arteriolar compartments is the local transmural pressure. Physiologically, both the pressure and flow contribute to the regulation of arterioles, with the pressure shown to be more important in cats mesentery [79]. When we used the transmural pressure as the input to the arterioles autoregulation, our simulations showed results more close to what we expected to be physiologically plausible.

Instead of calculating the smooth muscle tension as [9], we consider that the input variable passes directly trough a sigmoidal function followed by a low-pass filter, similar to [48]. To account for heterogeneous diameter changes along different vessel sizes, we considered different sigmoid functions based on data from experiments in cats [80]: $\boldsymbol{\sigma}_{Ar}(x)$ is used for the arteries compartment and $\boldsymbol{\sigma}_{Al}(x)$ which is used both for the arterioles and the microcirculation compartments. We make the distinction that the input for the arteriolar compartment is the transmural pressure while for the microcirculation it is the blood flow, to account for the metabolic mechanism on smaller vessels. They are shown in Fig 3 **(a)** and **(b)**. For the arterioles sigmoid we had to find a compromise between the agreement to data in [80] and physiological agreement of the results with experiments in humans (e.g. [3, 4, 9, 81]), so that the negative part of our $\boldsymbol{\sigma}_{Al}(x)$ is slightly steeper than in [28]. Its lower limit in the positive part was taken from [60].

During slight hypotension or hypertension, the diameter of the arteries change the most, while the arterioles remain almost unchanged. When MAP continues decreasing or increasing, the arteries' response saturate and the response of the arterioles increases dramatically [28], which is a behavior comparable to a sigmoid containing an initial threshold. The response of cerebral vessels to hypertension is lower than to hypotension [48].

We used the same sigmoid for both the arterioles and microcirculation, in which the terminal arterioles are comprised, because in [60] large arterioles and small arterioles display similar activation functions.

We do not account for the late dilation of the arterioles during extreme hypertension [80]. The upper and lower limits of the arteries sigmoid in Fig 3 **(a)** match very well with the diameter dilation and constriction in the order of 11% of the brachial artery in response to nitroglycerin and norepinephrine, respectively [82].

Baroreflex mechanism

Cerebral blood vessels are densely innervated with both sympathetic and parasympathetic nerve fibers [22]. The direct effect of sympathetic tone on cerebral vasculature is still not completely understood and varies highly over mammals [83]. In humans it is thought that baroreflex plays an important role in protecting the blood-brain barrier during acute hypertension, but in normal conditions it has little

Fig 3. Sigmoid functions for each of the regulated elements. (a): $\boldsymbol{\sigma}_{Ar}(x)$, used for the arteries. **(b)**: $\boldsymbol{\sigma}_{Al}(x) = \boldsymbol{\sigma}_{\mu_{circ}}(x)$, used for the arterioles and microcirculation. **(c)**: $\boldsymbol{\sigma}_{ECA}(x)$, used for the external carotid and extracranial arteries, adapted from [37]. **(d)**: $\boldsymbol{\sigma}_{HR}(x)$, used for the heart rate, taken from [37]. The central x corresponds to the baseline level for each of the mechanisms inputs. Note that the central x for $\boldsymbol{\sigma}_{HR}(x)$ is 1, whereas for the others is 0 because of different definitions of the inputs. See Eqs 54, 61, 68, 18 and 29 of S2 Appendix.

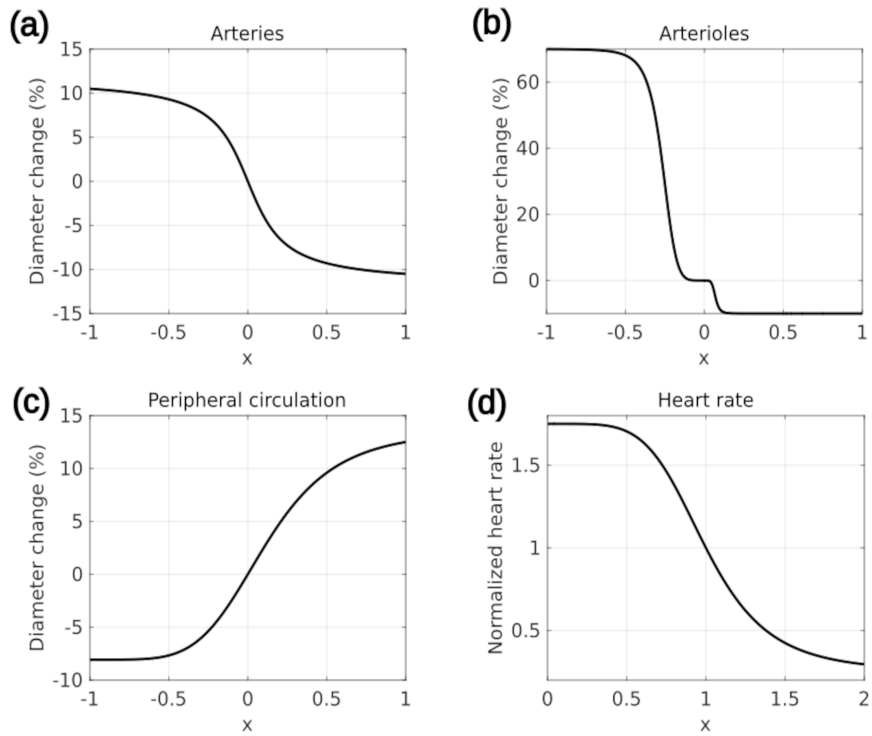

effect [2, 22]. We decided to neglect the direct effect of both sympathetic and parasympathetic tones on the cerebral vessels.

We consider that the baroreflex acts only on the diameter of the [ECA and ExAr] and at the HR. We compare the simulations in which the peripheral circulation of the head and neck is and is not controlled by sympathetic tone, because there is limited evidence supporting both cases, although recent work suggests that the ECA vascular bed is passive [4].

The ABP at the base of the common carotid compartment is an input to our model, which in terms of MAP is in open loop. In this way we could not model the complex MAP regulation in closed loop as in [36]. In future work it would be necessary to close the MAP loop including a model of the heart. The sigmoid functions used for the peripheral diameter change and HR, which were taken from [37], are shown in Fig 3 **(c)** and **(d)**.

Mathematical formulation

Fluid dynamics

We assume a simple linear equation for the pressure-induced fluid exchange between two communicating compartments:

$$p_{up} - p = \alpha f_{in} \,, \tag{1}$$

where p_{up} is the pressure of the upstream compartment, p is pressure of the actual compartment and f_{in} the flow rate entering the compartment. α is a constant resistance term for the passive vessels, and is a controlled variable for the peripheral compartment via baroreflex and for the intracranial autoregulated vessels. This is similar to Poiseuille flow where the blood is treated as an incompressible viscous fluid and α is inversely proportional to the fourth power of the vessel's diameter ($\alpha \propto \frac{1}{d^4}$), or equivalently ($\alpha \propto \frac{1}{A^2}$). However, here the baseline values for α's are not calculated from the Poiseuille equation, where $\alpha = \frac{8\pi\mu l}{A^2}$, but rather set to reproduce a physiologically valid pressure drop along the vessels and a normal steady-state CBF in the order of 12.5 ml/s.

The compartment's passive expansion or contraction in response to a change in the transmural pressure is modelled by a linear equation:

$$p_{lumen} - p_{brain} = E\left(\frac{A}{A_0} - 1\right) \,, \tag{2}$$

where E is the compartment's wall elastance, p_{lumen} is the vessel lumen pressure and p_{brain} is the brain parenchyma pressure on the corresponding side of the vessel. We remark that more detailed models of the human circulation such as [45] usually adopt a nonlinear equation.

Finally, we assert the principle of mass conservation:

$$l\frac{\partial A}{\partial t} = \sum_i f_i \,, \tag{3}$$

where f_i is the i'th flow entering or leaving the compartment. It f_i is entering, it is taken with positive sign. If it is leaving, it is taken with negative sign.

Cerebral autoregulation

We assume that each compartment's diameter (d) is given by $d = d_n(1 + \delta d)$, where d_n is its baseline value and δd is the normalized deviation from baseline. Therefore, in the non-regulated case we have $\delta d = 0$. In the regulated cases, d deviates from baseline. If for example the diameter doubles due to autoregulation we have $\delta d = 1$. For each of the controlled compartments we consider that its diameter deviates from baseline according to:

$$\tau_i \frac{\partial(\delta d_i)}{\partial t} + \delta d_i = \boldsymbol{\sigma}_i(x_i) \,, \quad i \in \{Ar, Al, \mu_{circ}\} \tag{4}$$

The sigmoid functions and the parameters are shown in Table 4.

For simplicity we chose to regulate only the vessel's resistance and its area at zero transmural pressure, but not the elastance. Physiologically, the elastance also changes when the vessels constrict or dilate. For example, [82] reported a statistically significant non-parallel shift in the pressure-area curves of the brachial artery in response both to a vasodilator and to a vasoconstrictor. Changing A_0 and not E corresponds to a parallel upward or downward shift of the linear Eq 2. Having δd from Eq 4, the vessel's cross-sectional area at zero transmural pressure follows from:

$$A_0 = A_{0n}(1 + \delta d)^2 \,, \tag{5}$$

Table 4. Parameters and their source for autoregulation controlled variables.

Variable	Input to autoregulation - x	Sigmoid function - $\boldsymbol{\sigma}(x)$	Time constant - τ (s)
Arteries diameter change (δd_{Ar})	Local transmural pressure	$\boldsymbol{\sigma}_{Ar}(x) = a \cdot arctan(b \cdot x)$, $a = -0.07497$, $b = 5.821$	3*
Arterioles diameter change (δd_{Al})	Local transmural pressure	$\boldsymbol{\sigma}_{Al}(x) = a\frac{1}{1+(x/k)^{-b}}$, $a = 0.7002$, $b = 5.63$, $k = -0.2655$, $x \leq 0$ $a = -0.1$, $b = 5.63$, $k = 0.0697$, $x > 0$	10**
Microcirculation diameter change ($\delta d_{\mu_{circ}}$)	Local blood flow	$\boldsymbol{\sigma}_{\mu_{circ}}(x) = \boldsymbol{\sigma}_{Al}(x)$	20 [28]

* is within the range reported in the literature for the myogenic effect [9, 29], ** was chosen as an intermediate value because fast and slow mechanisms act on arterioles. All the inputs contain an additional pure delay of 1 s for hypotension and 3 s for hypertension simulations due to an online FIR filter designed to estimate their mean values. We observed that the the model's CBF is highly dependent on the parameters in this Table. In future work they could be tuned to reproduce different autoregulation indexes such as in [84].

where A_{0n} is the vessel's baseline cross-sectional area at zero transmural pressure.

The regulated flow resistance follows from:

$$\alpha = \frac{\alpha_n}{(1+\delta d)^4}\,, \tag{6}$$

where α_n is the vessel's baseline flow resistance.

Baroreflex mechanism

The resistance and cross-sectional area at zero transmural pressure of the ECA and ExAr compartments are controlled by the baroreflex in the same manner as all other controlled vessels (Eqs 4, 5 and 6), trough the shift of their diameter from baseline that follow a sigmoid function ($\boldsymbol{\sigma}_{ECA}$) which was adapted from [37]:

$$\tau_{ECA}\frac{\partial(\delta d_{ECA})}{\partial t} + \delta d_{ECA} = \boldsymbol{\sigma}_{ECA}(x_{ECA}) \tag{7}$$

We assume that the normalized shifts from baseline at the ECA and extracranial arteries are equal: $\delta d_{ExAr} = \delta d_{ECA}$.

The normalized heart rate ($\widetilde{HR}$) active control by the baroreflex is assumed to be affected both by the sympathetic and parasympathetic tones, as in [37].

$$\tau_{HR}\frac{d\widetilde{HR}}{dt} + \widetilde{HR} = \boldsymbol{\sigma}_{HR}(x_{HR}) \tag{8}$$

$$\boldsymbol{\sigma}_{HR}(x) = \alpha_{HR} \cdot n_s(x) - \beta_{HR} \cdot n_p(x) + \gamma_{HR}\,, \tag{9}$$

where and α_{HR} and β_{HR} are respectively weights for the sympathetic and parasympathetic contributions. γ_{HR} is a constant that sets the normalized heart rate in baseline conditions equals to 1. The normalized sympathetic and parasympathetic neural activities are given by

$$n_s(x) = \frac{1}{1+x^{+\nu}} \tag{10}$$

$$n_p(x) = \frac{1}{1+x^{-\nu}} \tag{11}$$

The input x_{HR} is taken as $\frac{<p_{ExICA}>}{(p_{ExICA})_n}$, which is the ratio between the mean pressure at the extracranial ICA segment estimated by an online low-pass filter $< p_{ExICA} >$ and

the extracranial ICA normal pressure $(p_{ExICA})_n$. Finally, the absolute heart rate HR is given by

$$HR = \widetilde{HR} \cdot HR_n \,, \tag{12}$$

where $\widetilde{HR}$ is the normalized heart rate and HR_n is the baseline heart rate. The baroreflex parameters and their source are shown in Table 5.

Table 5. Parameters and their source for baroreflex controlled variables.

Variable	Input to baroreflex - x	Sigmoid function - $\boldsymbol{\sigma}(x)$ [37]	Time constant - τ (s)
Normalized heart rate ($\widetilde{HR}$)	Pressure at internal carotid (extracranial segment)	$\boldsymbol{\sigma}_{HR}(x) = \alpha_{HR} \cdot \frac{1}{1+x^{+\nu}} - \beta_{HR} \cdot \frac{1}{1+x^{-\nu}} + \gamma_{HR}$ $\alpha_{HR} = 1.75$, $\beta_{HR} = -0.25$, $\gamma_{HR} = 0$, $\nu = 5$	3 [37]
Peripheral arteries diameter change ($\delta d_{ExAr} = \delta d_{ECA}$)	Pressure at internal carotid (extracranial segment)	$\boldsymbol{\sigma}_{ECA}(x) = \left(\alpha_{ECA} \cdot \frac{1}{1+(x+1)^{+\nu}} + \gamma_{ECA}\right)^{\frac{-1}{4}} - 1$ $\alpha_{ECA} = 0.8$, $\gamma_{ECA} = 0.6$, $\nu = 5$	15 [36]

All the inputs contain an additional pure delay of 1 s for hypotension and 3 s for hypertension simulations due to an online FIR filter designed to estimate their mean values.

Online estimation of mean flows and pressures

We observed that the low-pass characteristics of the regulatory mechanisms alone were not able to properly filter the instantaneous values of their inputs. The shape of the mean values suffered alterations and high frequency components passed trough the mechanisms without enough attenuation, producing oscillations in their outputs.

We therefore designed a filter to online estimate the mean values of fluxes and pressures that served as inputs to the regulatory mechanisms. We picked a low-pass online finite impulse response (FIR) filter with cutoff frequency of 0.1 Hz and constant group delay (ϕ) of 1 s for hypotension and random simulations, which is the same initial delay found in rats kidneys vasodilation [29], and 3 s for hypertension simulations. The filter order (N) follows from $N = \frac{2\phi}{\Delta t}$, where Δt is the simulation time step in seconds. We calculated the filter coefficients using a Hamming window with length $N + 1$. The filter does not significantly slow the mechanisms because its cutoff frequency is in the order of twice that of the fastest regulatory mechanism ($\tau_{Ar} = 3$ s). It allows us to know precisely the pure delay (1 s for hypotension and random and 3 s for hypertension simulations) introduced to the regulatory inputs and it preserves the shape of the mean curves. The online filtered variables are denoted as $< . >$ in S2 Appendix.

Simulation setup

The model was implemented in Julia [85] v.1.5.2 as a differential-algebraic system of 120 equations. The derivatives were calculated using a first-order backward difference approximation and the system was solved step-by-step, the solution of the previous time step being the starting point for the next one. The time step was 0.01 s for the simulations of acute hypotension, random input and to study the effects of the arterial pressure wave, 0.05 s for hypertension and 0.1 s for the static autoregulation analysis. We used the nonlinear solver nlsolve() from the NLsolve.jl package.

Results

Acute hypotension

To investigate the effects of hypotension in situations corresponding to healthy and impaired conditions, we simulate bouts of acute hypotension by inputting the ABP (p_{init}) to the model, which drops according to the MAP fitted from published data in [3]:

$$MAP(t) = \begin{cases} \sum_{i=0}^{6} a_i (t - t_0)^i, & t_0 < t < t_0 + 60 \\ a_0, & \text{otherwise}\,, \end{cases} \tag{13}$$

where $t_0 = 20$ s is the start time of the acute bout of hypotension. $MAP(t)$ is given in mmHg and t in seconds. $(a_0, ..., a_6) = (102.40,\ -11.958,\ 1.4851,\ -7.4625 \cdot 10^{-2},\ 1.8273 \cdot 10^{-3},\ -2.1698 \cdot 10^{-5},\ 1.0033 \cdot 10^{-7})$.

The instantaneous ABP at the base of the CCA is given by:

$$p_{init}(t) = MAP(t) \left[1 + \sum_{n=1}^{8} a_n cos(n\omega x) + b_n sin(n\omega x) \right], \tag{14}$$

where $(a_1, ..., a_8) = (-0.0472,\ -0.0698,\ -0.0365,\ -0.0152,\ -0.0018,\ +0.0069,\ +0.0038,\ +0.0083)$, $(b_1, ..., b_8) = (+0.1378,\ +0.0389,\ -0.0219,\ -0.0096,\ -0.0238,\ -0.0056,\ -0.0057,\ +0.0007)$. Note that we account for the pulse pressure reduction in the same proportion as the change in MAP.

Using this input we perform three simulations:

(S_1) **Non-regulated**. All regulatory mechanisms are inactivated.

(S_2) **Regulated**. CA, baroreflex HR control and baroreflex peripheral circulation control at the ECA and ExAr peripheral compartments are activated.

(S_3) **Regulated excluding baroreflex at ECA vascular bed**. CA and baroreflex HR control are activated, but peripheral circulation control via baroreflex at the ECA and ExAr is inactivated.

In simulations S_2 and S_3, at the beginning of each heart beat we set $\omega = 2\pi \cdot HR$, where HR is the last value in Hz of the variable HR and ω is kept constant until the end of the heart beat. We do this to avoid discontinuities on the input pressure. The mean values in Figs 4 and 6 were calculated in post-processing using a 5th order low-pass Butterworth filter with cutoff frequency of 0.5 Hz that is applied forwards and backwards. From now on, unless otherwise stated, ICA compartment refers to the IcrICA compartment to simplify the notation.

Fig 4 shows the obtained $f_{ICA} = f_{IcrICA}$, which corresponds to CBF in our model, and f_{ECA}, which mimics the total blood flow to the peripheral circulation of the head and neck. CBF was rapidly reestablished in approximately 7.5 s with a small overshoot (2.24%) in the regulated simulations. The flow at the ECA compartment was prolongedly suppressed in comparison to the ICA compartment in the regulated simulations. The inclusion of baroreflex regulation at the extracranial vasculature in simulation S_2 had negligible effects on CBF regulation in comparison to the case in which CA is present but peripheral control is absent (S_3).

Fig 5 is a zoom of Fig 4, but shows the instantaneous flows at other compartments as well. We see the increase in HR and that CBF is much closer to baseline level in the regulated simulations.

Fig 6 shows the instantaneous values and the mean pressures for several compartments. We observed on one hand that the pressures at the ICA and arteries follow very closely the shape of the input p_{CCA} in all simulations. On the other hand,

Fig 4. Mean and instantaneous flow history at the internal carotid (panel (a) - ICA) and external carotid (panel (b) - ECA) compartments for the three regulated and non-regulated simulations (S_i) of bout of acute hypotension. S_1: non-regulated (no reg., dashed lines); S_2: regulated including cerebral autoregulation (CA), baroreflex heart rate (HR) control and baroreflex peripheral circulation control at ECA vascular bed (reg., solid lines); S_3: regulated excluding peripheral circulation control at ECA vascular bed, but including CA and baroreflex HR control (reg. exc. ECA, dotted lines). Mean blood flows are represented by thick lines and are denoted by $< . >$. The instantaneous pulsatile flows are only shown for simulation S_2. In our model the flow at ICA mimics the total cerebral blood flow (CBF) and the blood flow at ECA mimics the peripheral circulation of the head and neck. The figure shows a rapid reestablishment with a small overshoot (2.24%) of the ICA blood flow and a prolonged suppression of the ECA blood flow in the regulated simulations. The inclusion or exclusion of peripheral vasculature regulation at the ECA vascular bed via baroreflex had negligible effects on CBF. Abbreviation: Skin blood flow (SkBF).

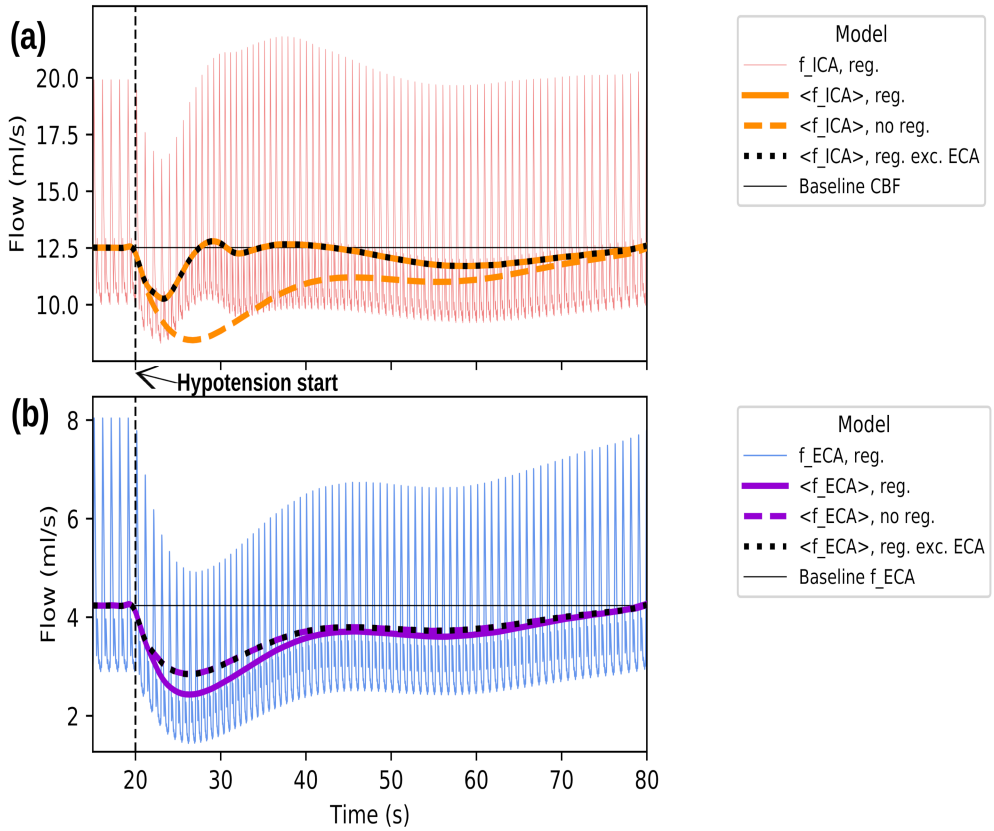

the pressures at the arterioles, microcirculation and brain parenchyma were highly affected by the autoregulation in the regulated simulations, returning to baseline levels much faster, with an overshoot in the microcirculation. The ICP presented an initial decrease followed by a small increase.

Fig 7 shows the flow resistance for each of the regulated compartments normalized by the corresponding baseline values and the HR during the bout of acute hypotension. The total cerebrovascular resistance is calculated by $\alpha_{total} = \alpha_{IcrICA} + 0.5(\alpha_{Ar} + \alpha_{Al} + \alpha_{\mu_{circ}} + \alpha_V) + \alpha_{vSinus} + \alpha_{out}$, which accounts for the resistances in series and in parallel. The total cerebrovascular resistance decreased

Fig 5. Instantaneous pulsatile flow dynamics in the regulated and non-regulated simulations (S_i) of bout of acute hypotension. Panel **(a)** shows regulated simulations (S_2 and S_3). S_2 includes cerebral autoregulation (CA), baroreflex heart rate (HR) control and baroreflex peripheral circulation control at external carotid (ECA) vascular bed (reg., solid lines); S_3 excludes peripheral circulation control at ECA vascular bed via baroreflex but includes CA and baroreflex HR control (reg. exc. ECA, dotted lines). Panel **(b)** shows S_1: non-regulated simulation in which all regulatory mechanisms inactivated (no reg.). The comparison between panels **(a)** and **(b)** shows that HR increased and CBF is much closer to the baseline level on the regulated simulations.

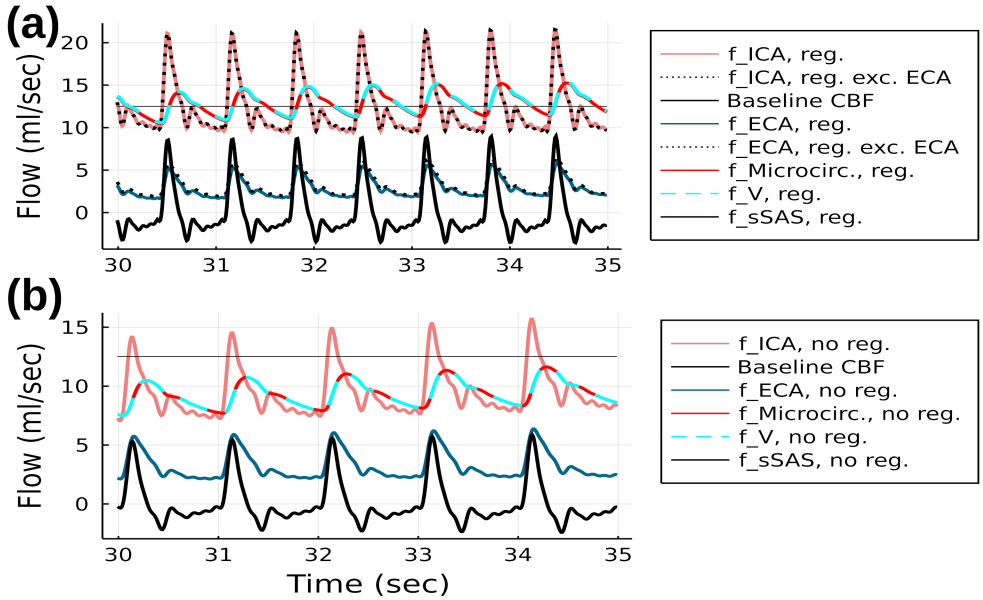

by 27.7% and the arterioles showed the greatest reduction in resistance in the regulated simulations. Baroreflex in simulation S_2 causes a change in the peripheral resistance in the opposite direction of the autoregulated brain vessels resistance.

Acute onset of hypertension

We also perform the three simulations (S_1: **Non-regulated**, S_2: **Regulated** and S_3: **Regulated excluding baroreflex at ECA vascular bed**) described in the previous section during an acute onset of hypertension. We input a MAP taken from published data in [86], which induced hypertension in rats by injecting kainic acid into the nucleus tractus solitarii. In order to make the input pressure more physiologically plausible to what is expected in humans, we re-scaled the data to set the baseline level equals to 102.40 mmHg and a maximum MAP of approximately 150 mmHg in the end of the hypertensive onset. The pulsatile Fourier coefficients were the same as in Eq 14.

The mean values in Figs 8 and 9 were calculated in post-processing using a 5th order low-pass Butterworth filter with cutoff frequency of 0.1 Hz that is applied forwards and backwards.

Fig 8 shows the obtained CBF and the blood flow to the extracranial vascular bed. We observed that during the non-regulated simulation, CBF largely exceeded a range of (Baseline CBF ±20%), which is an arbitrary definition of normal CBF range in [87]. During the regulated simulations, CBF was kept within normal ranges.

The pressures at the intracranial compartments shown in Fig 9 highlight that CA

Fig 6. Mean and instantaneous pressure history for the three regulated and non-regulated simulations (S_i) of bout of acute hypotension. S_1: non-regulated (no reg., dashed lines); S_2: regulated including cerebral autoregulation (CA), baroreflex heart rate (HR) control and baroreflex peripheral circulation control at external carotid (ECA) vascular bed (reg., solid lines); S_3: regulated including CA and baroreflex HR control, but excluding peripheral circulation control at ECA vascular bed (reg. exc. ECA, dotted lines). Mean pressures are represented by thick lines and are denoted by $< . >$. The pressure at the base of the common carotid (CCA) is an input to our model, but the HR is a controlled variable. The instantaneous pulsatile pressures are only shown for simulation S_2. We see that the pressure at the arterioles, microcirculation and brain parenchyma return much faster to baseline levels than the pressure at the arteries. Note the different scales of the vertical axis at the four panels. ICA: Internal carotid. ECA: External carotid. Ar: Arteries. Al: Arterioles. Microcirc.: Microcirculation. br: Brain. Lv: Lateral ventricles.

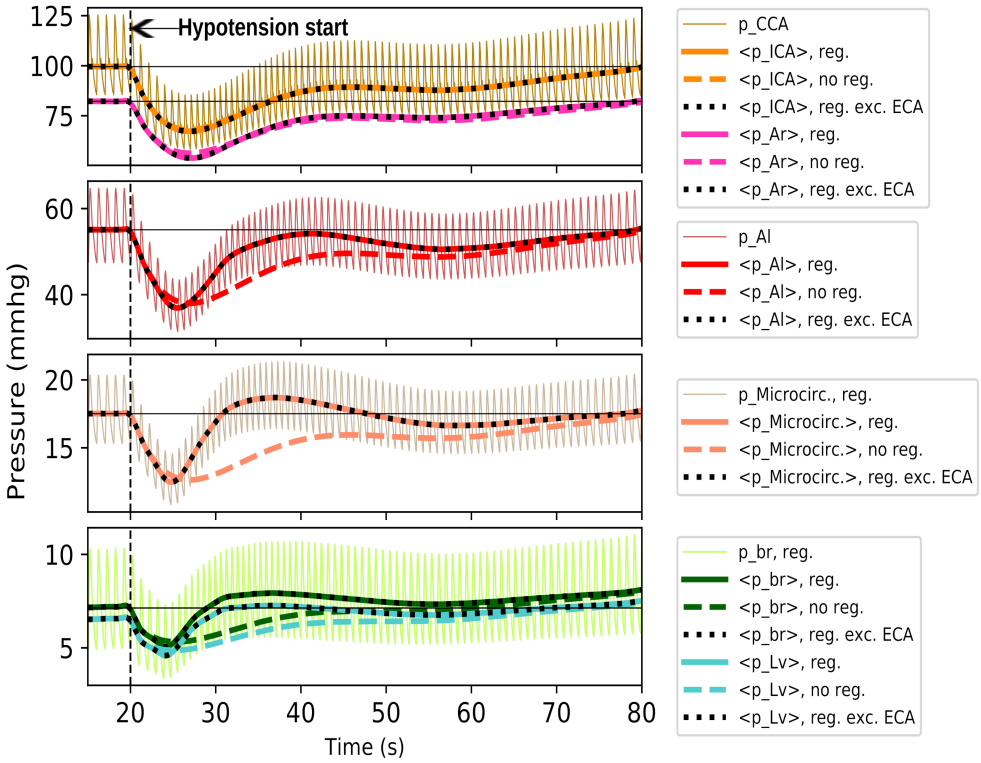

had a remarkable effect on keeping the pressure at the microcirculation much closer to the baseline level in comparison to larger vessels. The arteries, for example, were highly affected by the input pressure even in the regulated simulations.

Fig 10 shows the normalized flow resistances for each regulated compartment. We note that the arteries start to respond from the very beginning, even with small variations on the input pressure. The arterioles, on the contrary, display a threshold behavior since they are activated only after a moderate level of hypertension. Moreover, it is possible to note the different time constants for each compartment. For example, the microcirculation takes a much longer time to respond.

Fig 7. Normalized flow resistance of each of the regulated compartments and heart rate (HR) during acute hypotension for regulated simulations. S_2: regulated including cerebral autoregulation (CA), baroreflex HR control and baroreflex peripheral circulation control at external carotid (ECA) vascular bed (reg., solid lines); S_3: regulated including CA and baroreflex HR control, but excluding peripheral circulation control at ECA vascular bed (reg. exc. ECA, dotted lines and dashed line only for ECA resistance). **(a)**: Resistances of each regulated compartments shown in normalized units relative to baseline values. Total brain cerebrovascular resistance (green) is calculated by applying principles of resistances in series and in parallel. ECA: External carotid. Ar: Arteries. Al: Arterioles. Microcirc.: Microcirculation. **(b)**: HR response during acute hypotension due to baroreflex mechanism.

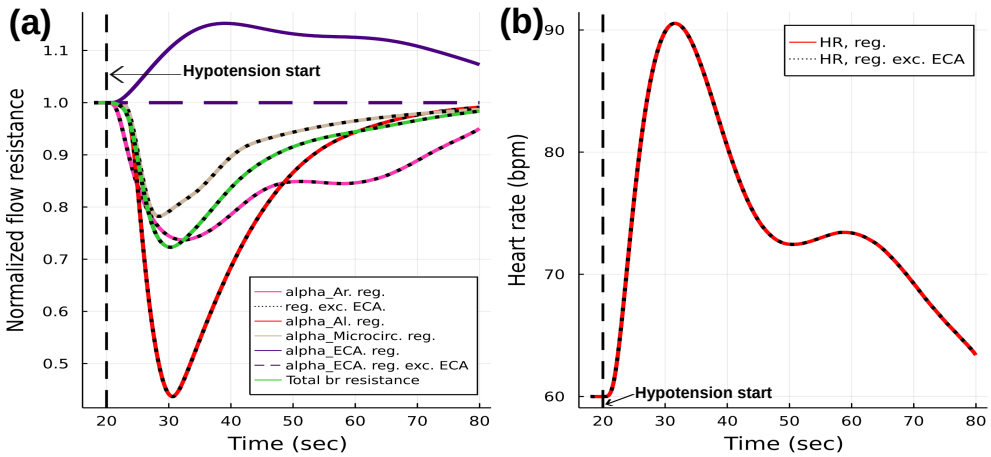

How much information does the extracranial blood flow carry about cerebral blood flow?

To answer this question, we performed the simulations below in addition to the hypotension and hypertension ones for each of the two cases: **Regulated**: CA and HR control are activated; **Non-regulated**: all control mechanisms are inactivated. The ECA vascular bed was considered passive in both cases in order to match with the discussions in [4].

- 3 simulations inputting random MAPs that follow random walks starting at 102.40 mmHg and whose increments are sampled from a Gaussian distribution with zero mean and standard deviation of 0.15 mmHg.

We then estimated the normalized conditional mutual information (NCMI $\in [0,1]$) [88] of the mean intracranial ($< f_{ICA} >=$ CBF) and extracranial ($< f_{ECA} >$) blood flows, conditioned on the mean input pressure ($< p_{init} >$). The conditioning on $< p_{init} >$ was chosen as an attempt to eliminate the effect of the arterial pressure on both the intracranial and extracranial blood flows.

$$\text{NCMI}(< f_{ICA} >, < f_{ECA} > | < p_{init} >) = \frac{I(< f_{ICA} >, < f_{ECA} > | < p_{init} >)}{\min\{H(< f_{ICA} > | < p_{init} >), H(< f_{ECA} > | < p_{init} >)\}}, \quad (15)$$

where $I(A, B|C)$ is the conditional mutual information between A and B, conditioned on C, and $H(A|C)$ is the entropy of A conditioned on C. The NCMI was calculated using entropies estimated by the finite sample correction method [89] in Python v.3.6 based on the MDEntropy library [90]. The estimated NCMI at each simulation is shown in Table 6. The mean flows and pressures were estimated using 5th order butterworth

Fig 8. Mean and instantaneous flow history at the internal carotid (panel (a) - ICA) and external carotid (panel (b) - ECA) compartments for the three regulated and non-regulated simulations of acute onset of hypertension. S_1: non-regulated (no reg., dashed lines); S_2: regulated including cerebral autoregulation (CA), baroreflex heart rate (HR) control and baroreflex peripheral circulation control at ECA vascular bed (reg., solid lines); S_3: regulated excluding peripheral circulation control at ECA vascular bed, and including CA and baroreflex HR control (reg. exc. ECA, dotted lines). Mean blood flows are represented by thick lines and are denoted by $< . >$. The instantaneous pulsatile flows are only shown for simulation S_2. In our model the flow at ICA mimics the total cerebral blood flow (CBF) and the blood flow at ECA mimics the peripheral circulation of the head and neck. In our model the inclusion or exclusion of peripheral vasculature regulation at the ECA vascular bed via baroreflex had negligible effects on CBF.

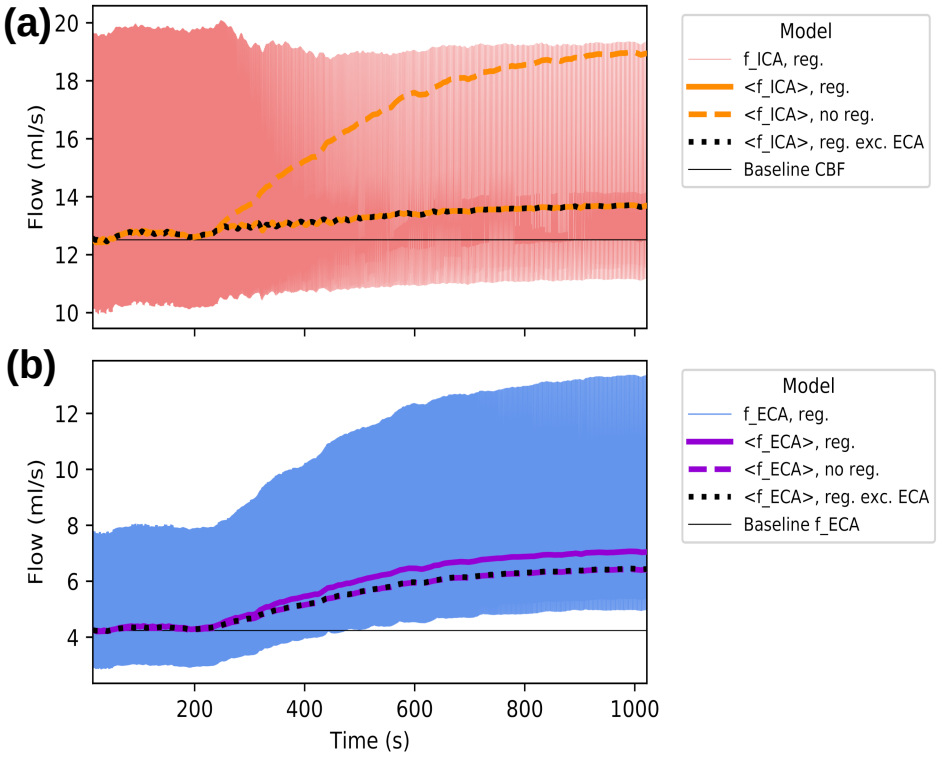

low-pass filters that are applied in both directions with cutoff frequencies of 0.5 Hz for the hypotension and random simulations, and 0.1 Hz for hypertension.

Table 6. Normalized conditional mutual information between CBF and the extracranial blood flow, conditioned on the input pressure.

	NCMI$(< f_{ICA} >, < f_{ECA} > \mid < p_{init} >)$	
Simulation	**Regulated**	**Non-regulated**
Hypotension	0.56	0.60
Hypertension	0.23	0.68
Random walk 1	0.33	0.50
Random walk 2	0.35	0.50
Random walk 3	0.36	0.49
Average± SD	0.37 ± 0.11	0.55 ± 0.08

Fig 9. Mean and instantaneous pressure history for the three regulated and non-regulated simulations of acute onset of hypertension. S_1: non-regulated (no reg., dashed lines); S_2: regulated including cerebral autoregulation (CA), baroreflex heart rate (HR) control and baroreflex peripheral circulation control at external carotid (ECA) vascular bed (reg., solid lines); S_3: regulated including CA and baroreflex HR control, but excluding peripheral circulation control at ECA vascular bed (reg. exc. ECA, dotted lines). Mean pressures are represented by thick lines and are denoted by $< . >$. The pressure at the base of the common carotid (CCA) is the input to our model, but the HR is a controlled variable. The instantaneous pulsatile pressures are only shown for simulation S_2. Note the different scales of the vertical axis at the four panels. ICA: Internal carotid. ECA: External carotid. Ar: Arteries. Al: Arterioles. Microcirc.: Microcirculation. br: Brain. Lv: Lateral ventricles.

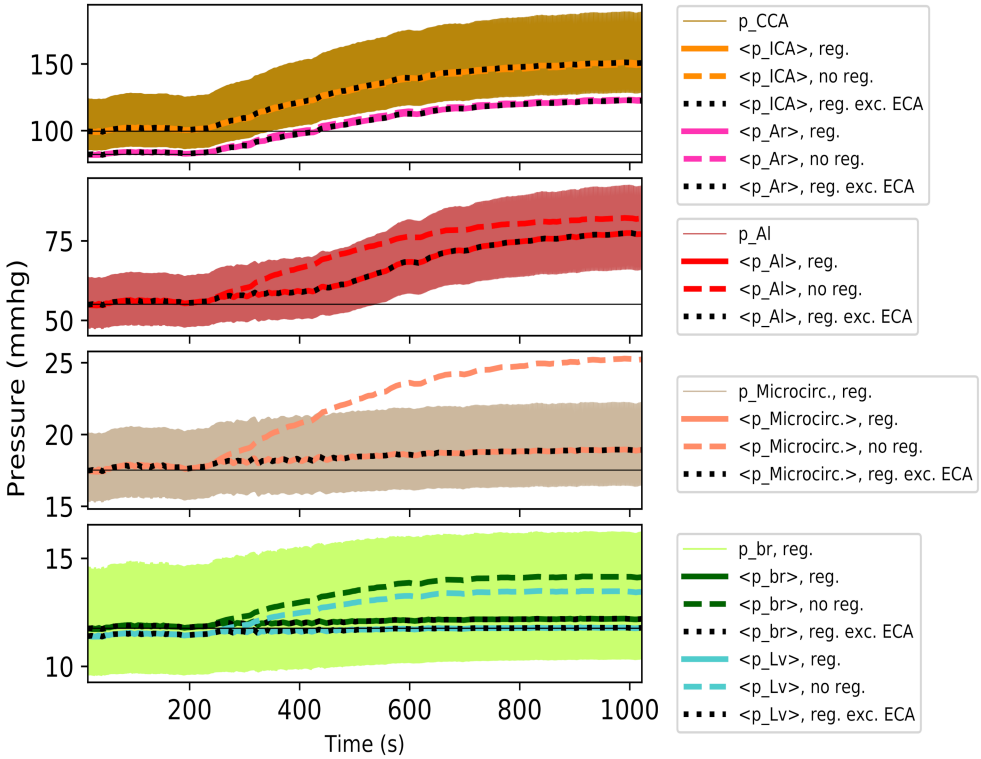

The obtained NCMI between CBF and the extracranial blood flow conditioned on the arterial pressure was modest on the regulated case (0.37 ± 0.11). It was particularly low for the hypertension simulation (0.23) and moderate for the hypotension (0.56). Note that the NCMI is a symmetric measure. The average NCMI was moderate (0.55 ± 0.08) on the non-regulated case.

Static autoregulation analysis

In order to analyse the proposed autoregulation mechanisms in steady-state, we performed simulations with various MAPs. MAP was maintained constant with zero pulse pressure throughout each simulation. We considered three situations:

(S_1) **All passive**. All regulatory mechanisms are inactivated.

(S_2) **Autoregulation only**. CA is activated, but HR and peripheral circulation control via baroreflex are inactivated.

Fig 10. Normalized flow resistance of each of the regulated compartments and heart rate (HR) during acute onset of hypertension for regulated simulations. S_2: regulated including cerebral autoregulation (CA), baroreflex HR control and baroreflex peripheral circulation control at external carotid (ECA) vascular bed (reg., solid lines); S_3: regulated including CA and baroreflex HR control, but excluding peripheral circulation control at ECA vascular bed (reg. exc. ECA, dotted lines and dashed line only for ECA resistance). **(a)**: Resistances of each regulated compartments shown in normalized units relative to baseline values. Total brain cerebrovascular resistance (green) is calculated by applying principles of resistances in series and in parallel. ECA: External carotid. Ar: Arteries. Al: Arterioles. Microcirc.: Microcirculation. **(b)**: HR response during acute onset of hypertension due to baroreflex mechanism.

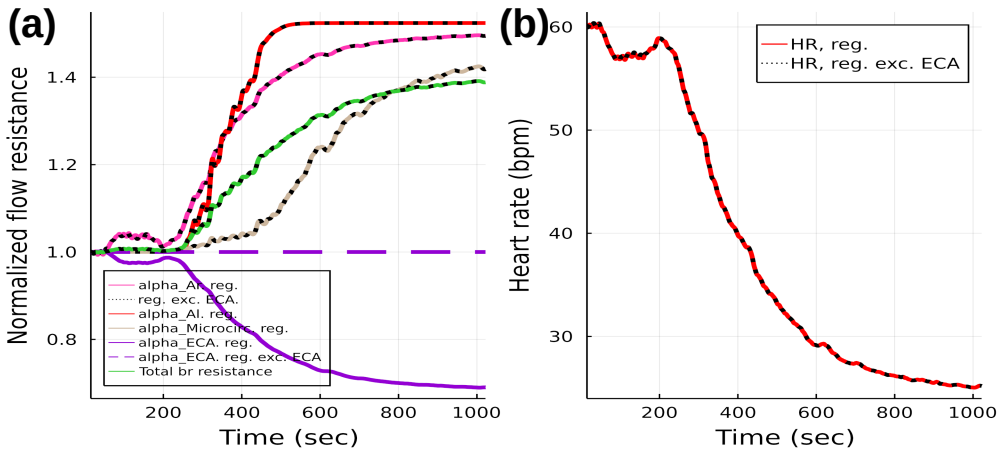

(S_3) **Autoregulation and peripheral vasculature control**. CA and peripheral circulation control at the ECA and ExAr via baroreflex are activated, but HR control is inactivated.

To achieve steady-state we run the system for about 5 times the largest time constant ($\tau_{\mu_{circ}} = 20$ s).

The pressure at the brain parenchyma is kept constant in the order of 7.1 mmHg to match the experimental setup in [80] and the analysis done in [28]. To do so we added a term in Eq 92 connecting both brain hemispheres to a compartment with infinite capacitance and constant pressure trough a low flow resistance.

Fig 11 shows the steady-state CBF in function of MAP for the three situations. We plot the range of normal CBF as (Baseline CBF $\pm 20\%$), the same arbitrary definition used in [87], which performed experiments in rats. By visual inspection of Fig 11, we obtained an MAP upper limit of autoregulation of 175 mmHg and a lower limit of 50 mmHg.

Effects of the arterial pressure wave on the model's intracranial dynamics

To answer the question of how the arterial pressure wave may affect the waveforms of the simulated pressures and flows, we fitted three input pressures from the high-fidelity aortic synthesized pressure waves in [19], which correspond to individuals aged 19, 42 and 83 years (S4 Appendix). They have increasing arterial stiffness, increasing arterial systolic and pulse pressures [19]. The fitted aortic pressures are shown in Fig 12 (top). For each subject we considered that the pressure at the base of the common carotid in

Fig 11. Static autoregulation curve - cerebral blood flow in function of mean arterial pressure in steady-state. Autoregulation curves are drawn for three simulations. S_1: All regulatory mechanisms are inactivated (all passive); S_2: Only CA is activated; S_3: CA and peripheral circulation control at ECA vascular bed are activated. At each simulation with different MAPs, MAP is kept constant with zero pulse pressure and the pressure at the brain parenchyma is kept constant at 7.1 mmHg by connecting each brain hemisphere to a compartment with constant pressure and infinite capacitance. Normal CBF range is shown as (Baseline CBF ±20%) which is an arbitrary definition to match [87]. We obtained 50 and 175 mmHg for the lower and upper limits of static autoregulation, respectively.

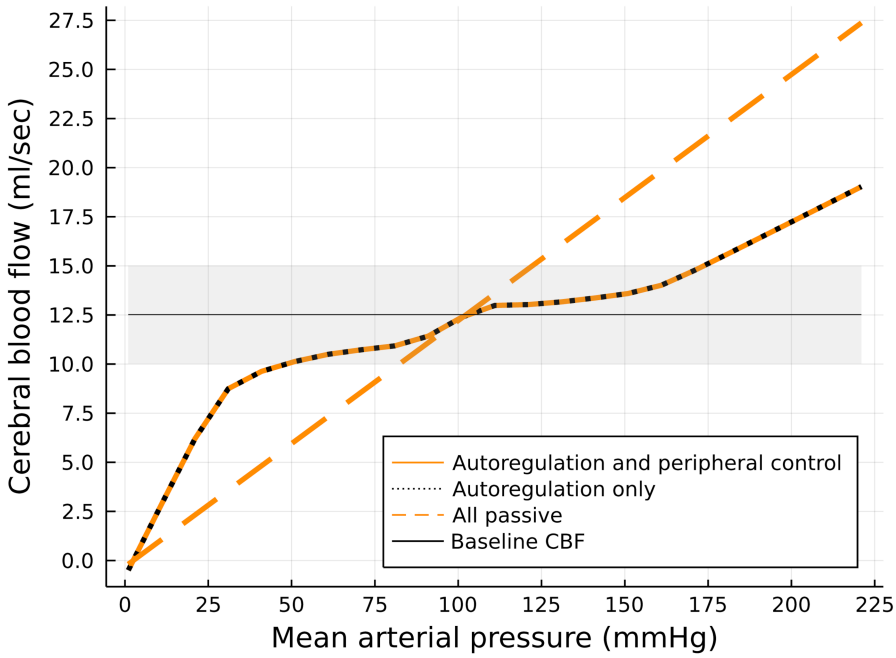

our model is the fitted aortic pressure. All regulatory mechanisms were inactivated because we assume that the individuals are in baseline conditions.

The simulated ICPs at the brain parenchyma are shown in Fig 12 (bottom). Accordingly to the arterial pressures, the obtained ICPs have increasing peak pressures and amplitudes as age increases. We observed that the model has a behavior similar to a low-pass filter if we consider that the input is the arterial pressure and the output is the ICP.

Fig 13 shows the simulated instantaneous cerebral blood inflow and outflow for the three subjects. The change in cerebral blood volume (CBV) is calculated using Eq 16:

$$\Delta CBV(t) = \int_0^t [F_a(t) - F_v(t)]\, dt\,, \tag{16}$$

where $F_a(t)$ is the total cerebral arterial inflow and $F_v(t)$ is the total cerebral venous outflow [20]. We see that the waveform of the change in CBV in Fig 13 is very similar to the ICP waveform in Fig 12.

Fig 12. Effects of the arterial pressure wave on the model's intracranial pressure (ICP) wave. Aortic pressure waves of individuals aging 19, 42 and 83 years fitted from [19] are set as the pressure at the base of common carotid artery, which is the input to the model (top). They have increasing arterial stiffness, increasing arterial systolic and pulse pressures. The obtained ICPs at the brain parenchyma (bottom) show that the ICP peak and amplitude increase according to the input. The model behaves similarly to a low-pass filter if we consider that the input is the arterial pressure and the output is the ICP.

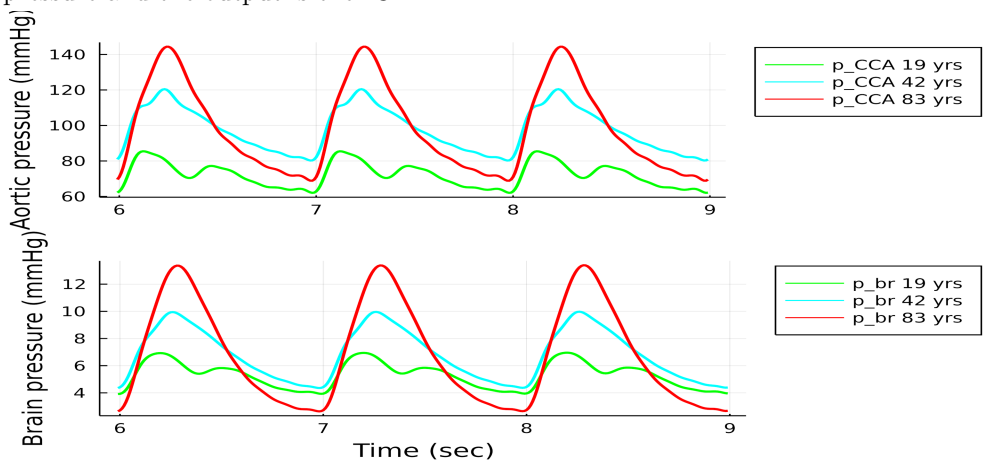

Fig 13. Effects of the arterial pressure wave on the model's intracranial blood flow dynamics. Total cerebral arterial inflow and total cerebral venous outflow obtained in our model for individuals aging 19, 42 and 83 years using input pressure waves fitted from [19]. The calculated change in cerebral blood volume (CBV) at each cardiac cycle has a waveform very similar to the intracranial pressure wave obtained in Fig 12 (bottom).

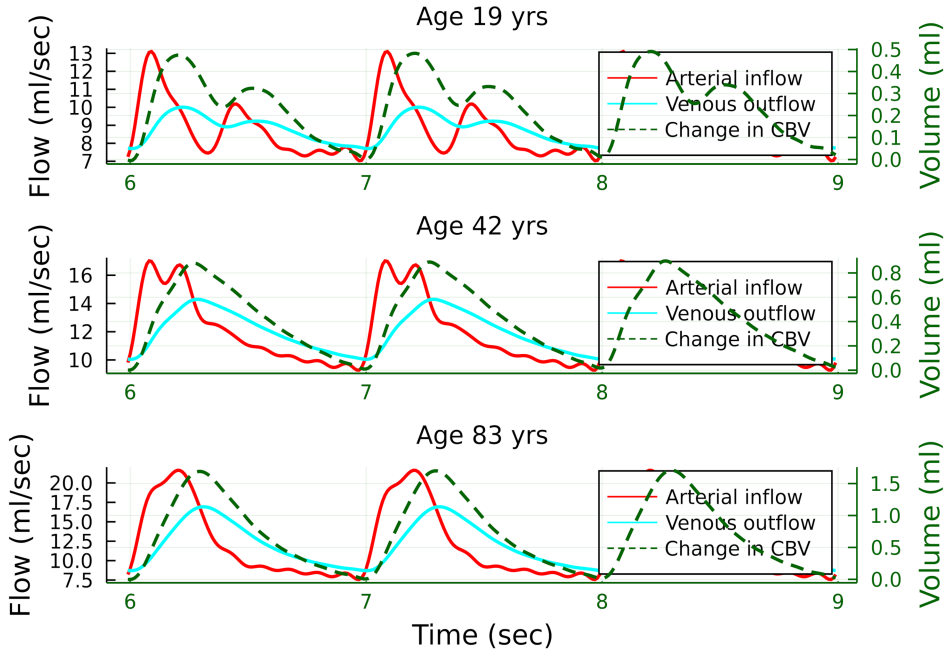

Discussion

Intracranial and extracranial dynamics during changes in MAP

The CBF dynamics in Fig 4 (top) is qualitatively in accordance with experiments from [3, 4, 9, 81, 84], which induced bouts of acute hypotension in humans. It initially decreased due to the change in MAP but was rapidly reestablished with a small overshoot. Note that [9] considered a visual stimulus in addition to the squat-stand maneuver, which might increase the demand for blood in the brain. The blood flow rate and blood flow velocity at the large cerebral arteries in [3, 4, 9, 81, 84] returned to baseline levels from 5 to 17 s after the start of the bout of acute hypotension. The return in 7.5 s of CBF in our model matches well with these times. Quantitatively, our overshoot was 21.6% and 5.9% smaller than those in [3] and [4]-control, respectively. We hypothesize that this is because our model includes the increase in HR, but not the increase in CO during acute hypotension. In [4] CO was found to be related to the increase in ICA blood flow, therefore likely related to dynamic CA.

The extracranial blood flow dynamics in Fig 4 (bottom) agrees with the dynamics reported in experiments in humans [3, 4]. The inclusion of vasoconstriction at the ECA vascular bed due to baroreflex in our model did not help reestablishing CBF during acute hypotension, given its negligible effects on CBF. This agrees with recent work suggesting that during acute hypotension the ECA vascular bed does not help reestablishing CBF in healthy young men [4]. The authors in [4] hypothesised that ECA blood flow may be regulated by a change in perfusion pressure regardless of sympathetic activity. Based on our results we raise the additional hypothesis that the ECA vascular bed may be regulated by sympathetic activity, but the effects of extracranial blood flow regulation on CBF are so small that [4] were not able to measure any significant influence of the ECA vascular bed on CBF regulation.

Here this behavior is likely because the ICA and ECA are in parallel and the input to our model is the pressure, not the blood flow at the CCA. This parallel arrangement with the pressure as an input may be physiologically valid, since MAP is regulated both in short and long terms and tissues in parallel are able to regulate their own blood flow, to a great extent, independently of flow to other tissues [91].

However, the negligible effects of the extracranial vascular bed on the intracranial blood flow regulation found in our model and in [4] must be carefully considered before any interpretation. If the input to the model were the CCA blood flow, any reduction in the ECA blood flow would imply an increase in the ICA blood flow of same value, in the case in which the input was kept constant. Therefore there would be a strong negative correlation between changes in ICA and ECA blood flow. [4] found a statistically significant moderate negative correlation ($r = 0.578$) between changes in ICA and ECA blood flow at only one time point (6 s after the start of the bout of acute hypotension) among 6 time points analysed.

This discussion is relevant because the extracranial vascular bed is more accessible. For example, if intracranial and extracranial blood flows are dynamically correlated, it may allow a less invasive assessment of the intracranial state by measuring external blood flow. Moreover, a better understanding of the relations between intracranial and extracranial hemodynamics may help improve methods such as functional Near-Infrared Spectroscopy and noninvasive ICP monitoring [8] whose measurements may be degraded by superficial tissue [5–7].

The authors in [92] found that after carotid endarterectomy, which reduces the flow resistance to the brain, the ECA blood flow reduced on average (5.1±48.2)% and the ICA blood flow increased on average (74.9±114.9)%. For most of the patients there was a concomitant reduction in the ECA blood flow and an increase in the ICA blood flow, although the authors did not perform correlation analysis between changes in the ECA

and ICA blood flow. The opposite behavior is observed when there is an increase in the ICA flow resistance. When the ICA is occluded, there may be an increase in the ECA blood flow and the ECA may contribute to CBF trough anastomotic channels [93]. This redistribution of blood flow occurs in longer timescales than the timescale of the acute hypotension experiments (e.g. in [3, 4]). Our simple arterial network is not able to depict complex interactions between the intracranial and extracranial vasculatures such as anastomotic channels.

During acute changes in MAP, the intracranial and extracranial blood flow dynamics are very different in healthy subjects because of regulatory mechanisms. Therefore, it is reasonable to expect that the intracranial and extracranial blood flows are weakly coupled. In our model they carry modest information about each other in such situations. However, when the autoregulation is impaired, the intracranial and extracranial blood flow dynamics become more similar.

The results in Fig 6 match with the protective role of CA to smaller vessels, since the pressures at the arterioles and microcirculation returned to baseline levels much faster than at the upstream compartments during acute hypotension. Similarly in Fig 9, the microcirculation was protected against a large increase in pressure on the regulated simulations of an acute onset of hypertension.

There is a lack of literature on the effects of acute hypotension to ICP in healthy subjects since such experiments cannot be ethically justified due to the invasiveness of the current methods to access the absolute value of ICP [94]. Therefore, it is difficult to validate our ICP results in Fig 6 with clinical data. In severely head-injured patients, the ICP decreased after the cuff deflation by an average of 5 mmHg, returning to baseline levels in 17 s followed by a late overshoot whose peak occurred 55 s after the maneuver in [95]. In [95] the MAP decreased by on average 19 $\pm$ 5 mmHg achieving its minimum 8 $\pm$ 7 seconds after the cuff deflation. Here our MAP decreases by 33.2 mmHg and the nadir occurs 6.9 s after the hypotension start.

The decrease of 27.7% in total cerebrovascular resistance (Fig 7) is comparable to data from experiments in humans. In [81] the total cerebrovascular resistance of 10 healthy subjects in response to a bout of acute hypotension decreased on average by 21.9% on hypocapnia, 24.1% on normocapnia and 21.5% on hypercapnia.

With respect to the static autoregulation curve (Fig 11), the overall shape on the autoregulated cases matches with the static autoregulation curve reported in the literature [12, 28, 87]. The upper limit of autoregulation of 175 mmHg matches very well with the 175 mmHg in [87]. Our lower limit of 50 mmHg was lower than the 80 mmHg in [87]. We remark that during extreme hypertension the curve in in [28] is steeper than ours, likely because we did not model the late dilation of the arterioles.

Effects of the arterial pressure wave on the intracranial dynamics

The change in CBF at each cardiac cycle (Fig 13) has a waveform similar to the ICP waveform in Fig 13 (bottom). This may illustrate the fact that the pulse pressure at the CSF, which is very close to the pulse pressure at the brain parenchyma, is governed by the pulsatile change in CBV and the craniospinal elastance [20]. Here the elastance coefficients are kept constant across all simulations. In future work, we might repeat these simulations with variable coefficients.

However, we observed that the ICP waveforms predicted by the model in Fig 12 (bottom) are also similar to the corresponding input arterial pressure waveforms in Fig 12 (top). In practice, such similarity is less pronounced. For example, in [94] a low correlation (0.28 $\pm$ 0.16) between the ICP and aortic pressure amplitudes was observed in idiopathic normal pressure hydrocephalus patients.

This similarity between the ICP and arterial pressure waves in the model is likely due to an unsuitability of the compartmental network to reproduce wave reflections [96] and complex dynamics in the arterial network, brain parenchyma and CSF systems, such as the shockwaves proposed by [97] to explain the mechanisms underlying the ICP wave.

Limitations

Our model has several limitations. We did not model the complex regulation of MAP via baroreflex in closed loop. Instead, just the HR and peripheral vasculature are controlled, whereas the ABP is an input to the model. Moreover, the direct effects of baroreflex on the cerebral vasculature were not included.

We did not calculate the separate contribution of each autoregulation mechanism, but rather we intended to grasp the main factors acting on each compartment. On top of that, we considered that the total flow resistance of the microcirculation, which comprises terminal arterioles, capillaries and venules, is affected by autoregulation. Physiologically, CA only acts up to capillaries.

Some limitations, such as the brain solid cell matrix surrounded by extracellular fluid assumption, are intrinsic to the Linninger model and are described in the seminal work [21].

Of note, considering that steady-state is achieved in about five times the largest time constant during the static autoregulation analysis is an approximation. It does not perfectly capture the model's state in very long timescales. In addition, long-term mechanisms were not modelled. For example, it is known in rats that baroreflex resets in about 48 h [98].

Finally, our experience showed that in simplified or moderately detailed models, higher agreement of model parameters to data reported in the literature for experiments in animals does not always mean more physiologically consistent results with experiments in humans. Often there is a need to find a compromise between the two.

Conclusions

The seminal model [21] comprises the most important systems of the intracranial dynamics, but was not designed to reproduce typical cerebral blood flow changes in response to changes in mean arterial pressure. We therefore added a cerebral autoregulation mechanism to account for the active vasodilation and vasoconstriction of brain vessels in response to changes in mean arterial pressure.

A limited baroreflex mechanism was included as a first step to model the joint contribution of both cerebral autoregulation and baroreflex to cerebral blood flow regulation. During regulated simulations of a bout of acute hypotension, cerebral blood flow returned rapidly to baseline level with a small overshoot, while the blood flow to the extracranial vascular bed suffered a prolonged suppression. These results agree with experiments in humans. The inclusion or exclusion of baroreflex control at the extracranial peripheral circulation had negligible effects on cerebral blood flow regulation, which supports recent work suggesting that the extracranial vascular bed is unrelated to cerebral blood flow regulation during acute hypotension in healthy young men [4].

In our model the pressures returned to baseline levels much faster at the arterioles, microcirculation and brain parenchyma than at the large arteries during acute hypotension, agreeing with the protective role of cerebral autoregulation to small vessels. Moreover, the extracranial blood flow carried modest information about cerebral blood flow in simulations where mean arterial pressure suffers dynamic changes and cerebral

autoregulation is intact. This information was higher in the simulations in which autoregulation is impaired.

Static autoregulation was also evaluated. The upper limit of autoregulation matched well with data from experiments in rats, while the lower limit was lower than the data. Future work needs to further evaluate the model's dynamic performance in direct comparison with clinical data both in normal and pathological cases, for example in subjects with impaired autoregulation. To simulate the impaired case, parameters in the model may be changed to decrease the regulatory gains and the intracranial compliance. Modeling the mean arterial pressure regulation in closed loop including a model of the heart is important in future work because cardiac output plays a role in regulating cerebral blood flow during acute hypotension. Finally, increasing the degree of detail of the arterial tree, possibly coupling 0D with 1D and 3D models of the largest vessels and cerebrospinal fluid compartments, may help us understand how several cerebral blood flow regulation mechanisms act together and influence the intracranial and extracranial dynamics.

Supporting information

S1 Appendix. Abbreviations and mathematical notation.

ABP	Arterial blood pressure
CBF	Cerebral blood flow
SkBF	Skin blood flow
CBV	Cerebral blood volume
CA	Cerebral autoregulation
CPP	Cerebral perfusion pressure
MAP	Mean arterial pressure
ICP	Intracranial pressure
CSF	Cerebrospinal fluid
SV	Stroke volume
CO	Cardiac output
HR	Heart rate
P_{xx}	Partial pressure
CCA	Common carotid artery
ICA	Internal carotid artery
ExICA	Internal carotid artery - extracranial segment
IcrICA	Internal carotid artery - intracranial segment
ECA	External carotid artery
Ex	Extracranial
Ar	Arteries
Al	Arterioles
Microcirc/ μ_{circ}	Microcirculation
V	Veins

vSinus	Venous sinus
Lv	Lateral ventricle
3V	Third ventricle
4V	Fourth ventricle
cSAS	Cranial subarachnoid space
sp.canal	Spinal subarachnoid space
br	Brain
br_{solid}	Brain solid cell matrix
br_{exf}	Brain extracellular fluid
p_{xx}	Pressure
$< . >$	Mean value using a low-pass filter
xx_n	Baseline value of variable xx
$xx^{L,R}$	Signifying two equations, one for the left brain hemisphere and one for the right brain hemisphere
xx^R	Right compartment
xx^L	Left compartment
$f_{xx_{in}}$	Flow into the compartment
$f_{xx_{out}}$	Flow out of the compartment

S2 Appendix. Equations.

Heart rate

$$\tau_{HR}\frac{d\widetilde{HR}}{dt} + \widetilde{HR} = \boldsymbol{\sigma}_{HR}(x_{HR})\,, \quad \text{normalized HR control via baroreflex} \tag{17}$$

$$x_{HR} = \frac{< p_{ExICA} >}{(p_{ExICA})_n}\,, \quad \text{input to baroreflex: pressure at ExICA} \tag{18}$$

$$HR = \widetilde{HR} \cdot HR_n\,, \quad \text{absolute value of heart rate} \tag{19}$$

Input pressure

$$p_{init} = MAP(t)\left[1 + \sum_n a_n cos(n\omega x) + b_n sin(n\omega x)\right]\,, \quad \text{pressure at base of CCA} \tag{20}$$

$$\omega = 2\pi HR\,, \quad \text{beat-to-beat fundamental frequency} \tag{21}$$

Common carotid artery (CCA)

$$l_{CCA}\frac{\partial A_{CCA}}{\partial t} = f_{CCA_{in}} - f_{CCA_{out}}\,, \quad \text{continuity} \tag{22}$$

$$p_{init} - p_{CCA} = \alpha_{CCA} f_{CCA_{in}}\,, \quad \text{momentum} \tag{23}$$

$$p_{CCA} - 0 = E_{CCA}\left(\frac{A_{CCA}}{A_{CCA0}} - 1\right)\,, \quad \text{distensibility} \tag{24}$$

External carotid artery (ECA)

$$l_{ECA}\frac{\partial A_{ECA}}{\partial t} = f_{ECA_{in}} - f_{ECA_{out}}\,, \quad \text{continuity} \tag{25}$$

$$p_{CCA} - p_{ECA} = \alpha_{ECA} f_{ECA_{in}}\,, \quad \text{momentum} \tag{26}$$

$$p_{ECA} - 0 = E_{ECA}\left(\frac{A_{ECA}}{A_{ECA0}} - 1\right)\,, \quad \text{distensibility} \tag{27}$$

$$\begin{cases} \tau_{ECA}\frac{\partial(\delta d_{ECA})}{\partial t} + \delta d_{ECA} = \boldsymbol{\sigma}_{ECA}(x_{ECA})\,, \text{ case in which baroreflex acts on ECA} \\ \delta d_{ECA} = 0\,, \text{case in which baroreflex does not act on ECA} \end{cases} \tag{28}$$

$$x_{ECA} = \frac{< p_{ExICA} >}{p_{ExICA_n}} - 1\,, \quad \text{input to baroreflex: pressure at ExICA} \tag{29}$$

$$\alpha_{ECA} = \frac{\alpha_{ECA_n}}{(1+\delta d_{ECA})^4}\,, \quad \text{controlled resistance} \tag{30}$$

$$A_{ECA0} = A_{ECA0n}(1+\delta d_{ECA})^2\,, \quad \text{controlled area} \tag{31}$$

Extracranial Arteries/Arterioles (ExAr)

$$l_{ExAr}\frac{\partial A_{ExAr}}{\partial t} = f_{ExAr_{in}} - f_{ExAr_{out}}\,, \quad \text{continuity} \tag{32}$$

$$p_{ECA} - p_{ExAr} = \alpha_{ExAr} f_{ExAr_{in}}\,, \quad \text{momentum} \tag{33}$$

$$p_{ExAr} - 0 = E_{ExAr}\left(\frac{A_{ExAr}}{A_{ExAr0}} - 1\right)\,, \quad \text{distensibility} \tag{34}$$

$$\alpha_{ExAr} = \frac{\alpha_{ExArn}}{(1+\delta d_{ECA})^4}\,, \quad \text{controlled resistance} \tag{35}$$

$$A_{ExAr0} = A_{ExAr0n}(1+\delta d_{ECA})^2\,, \quad \text{controlled area} \tag{36}$$

Extracranial Microcirculation (Exμ_{circ})

$$l_{Ex\mu_{circ}}\frac{\partial A_{Ex\mu_{circ}}}{\partial t} = f_{Ex\mu_{circ}in} - f_{Ex\mu_{circ}out}\,, \quad \text{continuity} \tag{37}$$

$$p_{ExAr} - p_{Ex\mu_{circ}} = \alpha_{Ex\mu_{circ}} f_{Ex\mu_{circ}in}\,, \quad \text{momentum} \tag{38}$$

$$p_{Ex\mu_{circ}} - 0 = E_{Ex\mu_{circ}}\left(\frac{A_{Ex\mu_{circ}}}{A_{Ex\mu_{circ}0}} - 1\right)\,, \quad \text{distensibility} \tag{39}$$

Extracranial Veins (ExV)

$$l_{ExV}\frac{\partial A_{ExV}}{\partial t} = f_{ExV_{in}} - f_{ExV_{out}}\,, \quad \text{continuity} \tag{40}$$

$$p_{ExAr} - p_{ExV} = \alpha_{ExV} f_{ExV_{in}}\,, \quad \text{momentum} \tag{41}$$

$$p_{ExV} - 0 = E_{ExV}\left(\frac{A_{ExV}}{A_{ExV0}} - 1\right)\,, \quad \text{distensibility} \tag{42}$$

$$p_{ExV} - p_{out} = \alpha_{out} f_{ExV_{out}}\,, \quad \text{additional momentum} \tag{43}$$

Extracranial internal carotid artery (ExICA)

$$l_{ExICA}\frac{\partial A_{ExICA}}{\partial t} = f_{ExICA_{in}} - f_{ExICA_{out}}\,, \quad \text{continuity} \tag{44}$$

$$p_{CCA} - p_{ExICA} = \alpha_{ExICA} f_{ExICA_{in}}\,, \quad \text{momentum} \tag{45}$$

$$p_{ExICA} - 0 = E_{ExICA}\left(\frac{A_{ExICA}}{A_{ExICA0}} - 1\right), \quad \text{distensibility} \tag{46}$$

Intracranial internal carotid artery (IcrICA)

$$l_{IcrICA}\frac{\partial A_{IcrICA}}{\partial t} = f_{IcrICA_{in}} - f_{IcrICA_{out}}\,, \quad \text{continuity} \tag{47}$$

$$p_{ExICA} - p_{IcrICA} = \alpha_{IcrICA} f_{IcrICA_{in}}\,, \quad \text{momentum} \tag{48}$$

$$p_{IcrICA} - 0.5(p^{R}_{br_{exf}} + p^{L}_{br_{exf}}) = E_{IcrICA}\left(\frac{A_{IcrICA}}{A_{IcrICA0}} - 1\right), \quad \text{distensibility} \tag{49}$$

Arteries

$$l^{L,R}_{Ar}\frac{\partial A^{L,R}_{Ar}}{\partial t} = {f_{Ar}}^{L,R}_{in} - {f_{Ar}}^{L,R}_{out}\,, \quad \text{continuity} \tag{50}$$

$$p_{ICA} - p^{L,R}_{Ar} = \alpha^{L,R}_{Ar}\,{f_{Ar}}^{L,R}_{in}\,, \quad \text{momentum} \tag{51}$$

$$p^{L,R}_{Ar} - p^{L,R}_{br_{exf}} = E_{Ar}\left(\frac{A^{L,R}_{Ar}}{{A_{Ar}}^{L,R}_{0}} - 1\right), \quad \text{distensibility} \tag{52}$$

$$\tau_{Ar}\frac{\partial(\delta d^{L,R}_{Ar})}{\partial t} + \delta d^{L,R}_{Ar} = \boldsymbol{\sigma}_{Ar}(x^{L,R}_{Ar})\,, \quad \text{autoregulation} \tag{53}$$

$$x^{L,R}_{Ar} = \frac{< p^{L,R}_{Ar} - p^{L,R}_{br_{exf}} >}{\left(p^{L,R}_{Ar} - p^{L,R}_{br_{exf}}\right)_n} - 1\,, \quad \text{input to autoregulation: transmural pressure} \tag{54}$$

$$\alpha^{L,R}_{Ar} = \frac{\alpha_{Arn}}{(1+\delta d^{L,R}_{Ar})^4}\,, \quad \text{controlled resistance} \tag{55}$$

$${A_{Ar}}^{L,R}_{0} = A_{Ar0n}(1+\delta d^{L,R}_{Ar})^2\,, \quad \text{controlled area} \tag{56}$$

Arterioles

$$l^{L,R}_{Al}\frac{\partial A^{L,R}_{Al}}{\partial t} = {f_{Al}}^{L,R}_{in} - {f_{Al}}^{L,R}_{out}\,, \quad \text{continuity} \tag{57}$$

$$p^{L,R}_{Ar} - p^{L,R}_{Al} = \alpha^{L,R}_{Al}\,{f_{Al}}^{L,R}_{in}\,, \quad \text{momentum} \tag{58}$$

$$p^{L,R}_{Al} - p^{L,R}_{br_{exf}} = E_{Al}\left(\frac{A^{L,R}_{Al}}{{A_{Al}}^{L,R}_{0}} - 1\right), \quad \text{distensibility} \tag{59}$$

$$\tau_{Al}\frac{\partial(\delta d^{L,R}_{Al})}{\partial t} + \delta d^{L,R}_{Al} = \boldsymbol{\sigma}_{Al}(x^{L,R}_{Al})\,, \quad \text{autoregulation} \tag{60}$$

$$x_{Al}^{L,R} = \frac{< p_{Al}^{L,R} - p_{br_{exf}}^{L,R} >}{\left(p_{Al}^{L,R} - p_{br_{exf}}^{L,R}\right)_n} - 1\,, \quad \text{input to autoregulation: transmural pressure} \tag{61}$$

$$\alpha_{Al}^{L,R} = \frac{\alpha_{Aln}}{(1+\delta d_{Al}^{L,R})^4}\,, \quad \text{controlled resistance} \tag{62}$$

$$A_{Al_0}{}^{L,R} = A_{Al0n}(1+\delta d_{Al}^{L,R})^2\,, \quad \text{controlled area} \tag{63}$$

Microcirculation (terminal arterioles, capillaries and venules)

$$l_{\mu_{circ}}^{L,R}\frac{\partial A_{\mu_{circ}}^{L,R}}{\partial t} = f_{\mu_{circ}in}{}^{L,R} - f_{\mu_{circ}out}{}^{L,R}\,, \quad \text{continuity} \tag{64}$$

$$p_{Al}^{L,R} - p_{\mu_{circ}}^{L,R} = \alpha_{\mu_{circ}}^{L,R} f_{\mu_{circ}in}{}^{L,R}\,, \quad \text{momentum} \tag{65}$$

$$p_{\mu_{circ}}^{L,R} - p_{br_{exf}}^{L,R} = E_{\mu_{circ}}\left(\frac{A_{\mu_{circ}}^{L,R}}{A_{\mu_{circ}0}{}^{L,R}} - 1\right)\,, \quad \text{distensibility} \tag{66}$$

$$\tau_{\mu_{circ}}\frac{\partial(\delta d_{\mu_{circ}}^{L,R})}{\partial t} + \delta d_{\mu_{circ}}^{L,R} = \boldsymbol{\sigma}_{\mu_{circ}}(x_{\mu_{circ}}^{L,R})\,, \quad \text{autoregulation} \tag{67}$$

$$x_{\mu_{circ}}^{L,R} = \frac{< f_{\mu_{circ}in}{}^{L,R} >}{\left(f_{\mu_{circ}in}{}^{L,R}\right)_n} - 1\,, \quad \text{input to autoregulation: blood flow} \tag{68}$$

$$\alpha_{\mu_{circ}}^{L,R} = \frac{\alpha_{\mu_{circ}n}}{(1+\delta d_{\mu_{circ}}^{L,R})^4}\,, \quad \text{controlled resistance} \tag{69}$$

$$A_{\mu_{circ}0}{}^{L,R} = A_{\mu_{circ}0n}(1+\delta d_{\mu_{circ}}^{L,R})^2\,, \quad \text{controlled area} \tag{70}$$

Veins

$$l_V^{L,R}\frac{\partial A_V^{L,R}}{\partial t} = f_V{}_{in}^{L,R} - f_V{}_{out}^{L,R}\,, \quad \text{continuity} \tag{71}$$

$$p_{\mu_{circ}}^{L,R} - p_V^{L,R} = \alpha_V^{L,R} f_V{}_{in}^{L,R}\,, \quad \text{momentum} \tag{72}$$

$$p_V^{L,R} - p_{br_{exf}}^{L,R} = E_V\left(\frac{A_V^{L,R}}{A_V{}_0^{L,R}} - 1\right)\,, \quad \text{distensibility} \tag{73}$$

Venous sinus

$$l_{vSinus}\frac{\partial A_{vSinus}}{\partial t} = f_{vSinus_{in}} - f_{vSinus_{out}}\,, \quad \text{continuity} \tag{74}$$

$$0.5(p_V^L + p_V^R) - p_{vSinus} = \alpha_{vSinus} f_{vSinus_{in}}\,, \quad \text{momentum} \tag{75}$$

$$p_{vSinus} - p_{out} = \alpha_{out} f_{vSinus_{out}}\,, \quad \text{additional momentum} \tag{76}$$

$$p_{vSinus} - 0.5(p_{br_{exf}}^L + p_{br_{exf}}^R) = E_V\left(\frac{A_{vSinus}}{A_{vSinus0}} - 1\right)\,, \quad \text{distensibility} \tag{77}$$

CSF system

Lateral ventricles

$$l_{Lv}^{L,R}\frac{\partial A_{Lv}^{L,R}}{\partial t} = f_{Lv_{in}}^{L,R} - f_{Lv_{out}}^{L,R}\,, \quad \text{continuity} \tag{78}$$

$$p_{Lv}^{L,R} - p_{3V} = \alpha_{3V} f_{Lv_{out}}^{L,R}\,, \quad \text{momentum} \tag{79}$$

$$p_{Lv}^{L,R} - p_{br_{exf}}^{L,R} = E_{Lv}^{L,R}\left(\frac{A_{Lv}^{L,R}}{A_{Lv_0}^{L,R}} - 1\right)\,, \quad \text{distensibility} \tag{80}$$

Third ventricle

$$l_{3V}\frac{\partial A_{3V}}{\partial t} = f_{3V_{in}} - f_{3V_{out}}\,, \quad \text{continuity} \tag{81}$$

$$p_{3V} - 0.5(p_{br_{exf}}^{L} + p_{br_{exf}}^{R}) = E_{3V}\left(\frac{A_{3V}}{A_{3V_0}} - 1\right)\,, \quad \text{distensibility} \tag{82}$$

Fourth ventricle

$$l_{4V}\frac{\partial A_{4V}}{\partial t} = f_{4V_{in}} - f_{4V_{out}}\,, \quad \text{continuity} \tag{83}$$

$$p_{3V} - p_{4V} = \alpha_{4V} f_{4V_{in}}\,, \quad \text{momentum} \tag{84}$$

$$p_{4V} - 0.5(p_{br_{exf}}^{L} + p_{br_{exf}}^{R}) = E_{4V}\left(\frac{A_{4V}}{A_{4V_0}} - 1\right)\,, \quad \text{distensibility} \tag{85}$$

Cranial subarachnoid space

$$l_{cSAS}\frac{\partial A_{cSAS}}{\partial t} = f_{cSAS_{in}} - f_{cSAS_{out}}\,, \quad \text{continuity} \tag{86}$$

$$p_{4V} - p_{cSAS} = \alpha_{cSAS} f_{cSAS_{in}}\,, \quad \text{momentum} \tag{87}$$

$$p_{cSAS} - 0.5(p_{br_{exf}}^{L} + p_{br_{exf}}^{R}) = E_{cSAS}\left(\frac{A_{cSAS}}{A_{cSAS_0}} - 1\right)\,, \quad \text{distensibility} \tag{88}$$

Spinal subarachnoid space

$$l_{sp.canal}\frac{\partial A_{sp.canal}}{\partial t} = f_{sp.canal_{in}} - f_{sp.canal_{out}}\,, \quad \text{continuity} \tag{89}$$

$$p_{cSAS} - p_{sp.canal} = \alpha_{sp.canal} f_{sp.canal_{in}}\,, \quad \text{momentum} \tag{90}$$

$$p_{sp.canal} - 0 = E_{sp.canal}\left(\frac{A_{sp.canal}}{A_{sp.canal_0}} - 1\right)\,, \quad \text{distensibility} \tag{91}$$

Brain parenchyma

$$f_{br_{exf}}{}_{in}^{L,R} - f_{br_{exf}}{}_{out}^{L,R} = 0\,, \quad \text{continuity} \tag{92}$$

$$f_{br_{exf}}{}_{in}^{L,R} = S_{const_{\mu_{circ}\to br}}^{L,R} + S_{\mu_{circ}\to br}^{L,R} \tag{93}$$

$$f_{br_{exf}}{}_{out}^{L,R} = S_{const_{br\to Lv}}^{L,R} + S_{br\to Lv}^{L,R} \tag{94}$$

$$p^{L,R}_{\mu_{circ}} - p^{L,R}_{br_{exf}} = \alpha_{\mu_{circ}\to br} S^{L,R}_{\mu_{circ}\to br}\,, \quad \text{momentum} \tag{95}$$

$$p^{L,R}_{br_{exf}} - p^{L,R}_{Lv} = \alpha_{br\to Lv} S^{L,R}_{br\to Lv}\,, \quad \text{momentum} \tag{96}$$

$$S^{L,R}_{const_{\mu_{circ}\to br}} = 0.0005 \text{ ml/s} \tag{97}$$

$$S^{L,R}_{const_{br\to Lv}} = 0.0005 \text{ ml/s} \tag{98}$$

Monro-Kellie doctrine is enforced separetely at each side of the skull:

$$\begin{aligned} V^{L,R}_{total_{intracranial}} = \text{constant} \Rightarrow \\ (0.5V_{IcrICA} + V^{L,R}_{Ar} + V^{L,R}_{Al} + V^{L,R}_{\mu_{circ}} + V^{L,R}_{V} + V_{vSinus}) \\ + (V^{L,R}_{Lv} + 0.5V_{3V} + 0.5V_{4V} + 0.5V_{cSAS}) + (V^{L,R}_{br_{solid}} + V^{L,R}_{br_{exf}}) = \text{constant} \end{aligned} \tag{99}$$

Equations connecting the compartments and source terms

$$f_{CCA_{out}} = f_{ExICA_{in}} + f_{ECA_{in}} \tag{100}$$

$$f_{ECA_{out}} = f_{ExAr_{in}} \tag{101}$$

$$f_{ExAr_{out}} = f_{Ex\mu_{circ}{}_{in}} \tag{102}$$

$$f_{Ex\mu_{circ}{}_{out}} = f_{ExV_{in}} \tag{103}$$

$$f_{ExICA_{out}} = f_{IcrICA_{in}} \tag{104}$$

$$f_{IcrICA_{out}} = f_{Ar}{}^{L}_{in} + f_{Ar}{}^{R}_{in} \tag{105}$$

$$f_{Ar}{}^{L,R}_{out} = f_{Al}{}^{L,R}_{in} \tag{106}$$

$$f_{Al}{}^{L,R}_{out} = f_{\mu_{circ}}{}^{L,R}_{in} \tag{107}$$

$$f_{\mu_{circ}}{}^{L,R}_{out} = f_{Lv}{}^{L,R}_{in} + f_{br_{exf}}{}^{L,R}_{in} + f_{V}{}^{L,R}_{in} \tag{108}$$

$$f_{vSinus_{in}} = f_{V}{}^{L}_{out} + f_{V}{}^{R}_{out} + f_{reabsorption} \tag{109}$$

$$f_{Lv}{}^{L,R}_{in} = S^{L,R}_{const_{\mu_{circ}\to Lv}} \tag{110}$$

$$S^{L,R}_{const_{\mu_{circ}\to Lv}} = 0.003 \text{ ml/s} \tag{111}$$

$$f_{3V_{in}} - f_{Lv}{}^{L}_{out} - f_{Lv}{}^{R}_{out} = f_{br_{exf}}{}^{L}_{out} + f_{br_{exf}}{}^{R}_{out} \tag{112}$$

$$f_{4V_{in}} = f_{3V_{out}} \tag{113}$$

$$f_{4V_{out}} = f_{cSAS_{in}} \tag{114}$$

$$f_{cSAS_{out}} = f_{sp.canal_{in}} + f_{reabsorption} \tag{115}$$

$$f_{reabsorption} = k(p_{cSAS} - p_{vSinus}) \tag{116}$$

$$1/k = 15.62 \text{ mmHg·min/ml} \tag{117}$$

$$f_{sp.canal_{out}} = 0 \tag{118}$$

$$p_{out} = 2.5 \text{ mmHg, zero amplitude} \tag{119}$$

$$\alpha_{out} = 0.0809088 \text{ mmHg·s/ml} \tag{120}$$

S3 Appendix. Constants used in the model.

Table 7. Baseline values used in the model for each compartment.

Compartment	Length (cm)	Area at rest (cm^2)	Elastance (mmHg)	Resistance (mmHg·s/ml)
Common carotid	(12.14 + 8.13)/2*	0.5765*	1600	0.04854525*
External carotid	6.10*	0.3223*	800000*	0.1220*
Extracranial arteries	6.16*	12.29*	1920	6.433*
Extracranial microcirculation	0.2730*	122.6*	6800	13.638*
Extracranial veins	7.473*	17.23*	756.56	3.1104*
Extracranial internal carotid	8.6*	0.3947*	800	0.0786*
Intracranial internal carotid	9.1*	0.1973*	1600	0.0831*
Arteries	4.15	3.42	1920	2.76912
Arterioles	1.75	4.74	410.28	4.33831545
Microcirculation	0.2618	38.0	6800	6.002803222
Veins	7.165	5.3388	756.56	2.078301471
Venous sinus	15.0	0.86	90.007	0.161896
Lateral ventricles	0.75	12.0	10.0	500.0 ($\alpha_{br \to Lv}$)
Third ventricle	1.0	2.5	10.0	1.0
Fourth ventricle	1.0	3.5	10.0	1.0
Cranial subarachnoid space	1.69	17.7658	80.0	1.0
Spinal cord	43.0	2.0	300.0	0.1
Brain extracellular fluid	7.0	30.0	———	8152.42 ($\alpha_{\mu_{circ} \to br}$)
Brain solid cell matrix	7.0	70.0	———	———

All parameters with the exception of * were taken from published and unpublished data in [21].

S4 Appendix. Aortic pressure waves fitted from [19] for individuals aging 19, 42 and 83 years.

$$p_{init} = a_0 + \sum_{n=1}^{8} a_n cos(n\omega x) + b_n sin(n\omega x)$$

Table 8. Baseline values for pressures, flows and HR used at hypotension and hypertension simulations.

Parameter	Hypotension	Hypertension
CBF = f_{ICA_n}	12.518 ml/s	12.515 ml/s
$(p_{ExICA})_n$	100.591 mmHg	100.599 mmHg
$\left(p_{Ar}^{L,R} - p_{br_{exf}}^{L,R}\right)_n$	75.085 mmHg	70.464 mmHg
$\left(p_{Al}^{L,R} - p_{br_{exf}}^{L,R}\right)_n$	47.935 mmHg	43.317 mmHg
$\left(f_{\mu_{circ}in}^{L,R}\right)_n$	6.256 ml/s	6.257 ml/s
HR_n	1 Hz = 60 bpm	1 Hz = 60 bpm
$p_{br_{exf}}^{L,R}$	7.133 mmHg	11.766 mmHg

Age (years)	Pressure wave Fourier coefficients [mmHg]
19	$(a_0, ..., a_8) = (+72.805, -1.7232, -0.2418, -3.7949, -0.9176, -1.0510, -0.9843, -0.3240, -0.4260)$ $(b_1, ..., b_8) = (+7.0992, +5.0640, +0.9592, -0.2273, +0.4517, -0.3920, -0.2460, -0.1824)$
42	$(a_0, ..., a_8) = (+98.529, -4.2922, -4.9021, -2.4110, -0.8043, -0.7461, -1.3538, -0.8557, -0.3375)$ $(b_1, ..., b_8) = (+16.0276, +3.586, +0.5741, +0.3451, +0.8614, +0.3377, -0.4699, -0.3575)$
83	$(a_0, ..., a_8) = (+99.341, -8.0572, -12.1456, -3.1937, -0.7437, -1.2039, -1.2926, -0.5074, -0.5952)$ $(b_1, ..., b_8) = (+ 31.713, +3.1270, -1.6578, -0.0335, + 0.6687, -0.2084, -0.3016, -0.1075)$

Acknowledgments

We thank professor Roland Köberle for comments and suggestions on the manuscript. Fig 2 created with BioRender.com.

References

1. Rivera-Lara L, Zorrilla-Vaca A, Geocadin RG, Healy RJ, Ziai W, Mirski MA. Cerebral autoregulation-oriented therapy at the bedside a comprehensive review. Anesthesiology. 2017;126(6):1187–1199. doi:10.1097/ALN.0000000000001625.

2. Ogoh S, Tarumi T. Cerebral blood flow regulation and cognitive function: a role of arterial baroreflex function. Journal of Physiological Sciences. 2019;69(6):813–823. doi:10.1007/s12576-019-00704-6.

3. Ogoh S, Lericollais R, Hirasawa A, Sakai S, Normand H, Bailey DM. Regional redistribution of blood flow in the external and internal carotid arteries during acute hypotension. American Journal of Physiology - Regulatory Integrative and Comparative Physiology. 2014;306(10):747–751. doi:10.1152/ajpregu.00535.2013.

4. Ogoh S, Sørensen H, Hirasawa A, Sasaki H, Washio T, Hashimoto T, et al. Dynamic cerebral autoregulation is unrelated to decrease in external carotid artery blood flow during acute hypotension in healthy young men. Experimental Physiology. 2016;101(8):1040–1049. doi:10.1113/EP085772.

5. Tachtsidis I, Scholkmann F. False positives and false negatives in functional near-infrared spectroscopy: issues, challenges, and the way forward. Neurophotonics. 2016;3(3):031405. doi:10.1117/1.nph.3.3.031405.

6. Caldwell M, Scholkmann F, Wolf U, Wolf M, Elwell C, Tachtsidis I. Modelling confounding effects from extracerebral contamination and systemic factors on functional near-infrared spectroscopy. NeuroImage. 2016;143:91–105. doi:10.1016/j.neuroimage.2016.08.058.

7. Milej D, Abdalmalak A, Rajaram A, St Lawrence K. Direct assessment of extracerebral signal contamination on optical measurements of cerebral blood flow, oxygenation, and metabolism. Neurophotonics. 2020;7(04):1–17. doi:10.1117/1.nph.7.4.045002.

8. Gomes I, Shibaki J, Padua B, Silva F, Gonçalves T, Spavieri-Junior DL, et al. Comparison of Waveforms Between Noninvasive and Invasive Monitoring of Intracranial Pressure. 2021; p. 135–140.

9. Spronck B, Martens EGHJ, Gommer ED, van de Vosse FN. A lumped parameter model of cerebral blood flow control combining cerebral autoregulation and neurovascular coupling. American Journal of Physiology - Heart and Circulatory Physiology. 2012;303(9). doi:10.1152/ajpheart.00303.2012.

10. Meyer JS, Handa J, Huber P, Yoshida K. Effect of Hypotension on Internal and External Carotid Blood Flow. Journal of Neurosurgery. 1965;23(2):191–198. doi:10.3171/jns.1965.23.2.0191.

11. Savin E, Siegelova J, Fisher B, Bonnin P. Intra- and extracranial artery blood velocity during a sudden blood pressure decrease in humans. European Journal of Applied Physiology and Occupational Physiology. 1997;76(3):289–293. doi:10.1007/s004210050250.

12. Ursino M, Giannessi M. A model of cerebrovascular reactivity including the circle of Willis and cortical anastomoses. Annals of Biomedical Engineering. 2010;38(3):955–974. doi:10.1007/s10439-010-9923-7.

13. Hlatky R, Furuya Y, Valadka AB, Gonzalez J, Chacko A, Mizutani Y, et al. Dynamic autoregulatory response after severe head injury. Journal of Neurosurgery. 2002;97(5):1054–1061. doi:10.3171/jns.2002.97.5.1054.

14. Czosnyka M, Miller C, Le Roux P, Menon DK, Vespa P, Citerio G, et al. Monitoring of Cerebral Autoregulation. Neurocritical Care. 2014;21(2):95–102. doi:10.1007/s12028-014-0046-0.

15. Reilly P, Bullock R, Piper I. Intracranial pressure and elastance. Head Injury 2Ed. 2005;(May):93–112. doi:10.1201/b13492-7.

16. Ebert T, Muzi M, Berens R, Goff D, Kampine J. Sympathetic Responses to Induction of Anesthesia in Humans with Propofol or Etomidate. Anesthesiology. 1992;76(5):725–733. doi:10.1097/00000542-199205000-00010.

17. Cheng LT, Tang LJ, Cheng L, Huang HY, Wang T. Limitation of the augmentation index for evaluating arterial stiffness. Hypertension Research. 2007;30(8):713–722. doi:10.1291/hypres.30.713.

18. Shirwany NA, Zou MH. Arterial stiffness: A brief review. Acta Pharmacologica Sinica. 2010;31(10):1267–1276. doi:10.1038/aps.2010.123.

19. Nichols WW. Clinical measurement of arterial stiffness obtained from noninvasive pressure waveforms. American Journal of Hypertension. 2005;18(1 SUPPL.):3–10. doi:10.1016/j.amjhyper.2004.10.009.

20. Avezaat C, van Eijndhoven JHM. Cerebrospinal fluid pulse pressure and craniospinal dynamics : a theoretical, clinical and experimental study [PhD Thesis]. Erasmus University Rotterdam, The Hague : Jongbloed; 1984. Available from: `http://hdl.handle.net/1765/38457`.

21. Linninger AA, Xenos M, Sweetman B, Ponkshe S, Guo X, Penn R. A mathematical model of blood, cerebrospinal fluid and brain dynamics. Journal of Mathematical Biology. 2009;59(6):729–759. doi:10.1007/s00285-009-0250-2.

22. Faraci FM, Heistad DD. Regulation of the cerebral circulation: Role of endothelium and potassium channels. Physiological Reviews. 1998;78(1):53–97. doi:10.1152/physrev.1998.78.1.53.

23. Ibrahim J, McGee A, Graham D, McGrath JC, Dominiczak AF. Sex-specific differences in cerebral arterial myogenic tone in hypertensive and normotensive rats. American Journal of Physiology - Heart and Circulatory Physiology. 2006;290(3):1081–1089. doi:10.1152/ajpheart.00752.2005.

24. Halpern W, Osol G, Coy GS. Mechanical behavior of pressurized in vitro prearteriolar vessels determined with a video system. Annals of Biomedical Engineering. 1984;12(5):463–479. doi:10.1007/BF02363917.

25. Ainslie PN, Duffin J. Integration of cerebrovascular CO2 reactivity and chemoreflex control of breathing: Mechanisms of regulation, measurement, and interpretation. American Journal of Physiology - Regulatory Integrative and Comparative Physiology. 2009;296(5). doi:10.1152/ajpregu.91008.2008.

26. Silverman A, Petersen NH. Physiology, Cerebral Autoregulation. StatPearls [Internet]. Treasure Island (FL): StatPearls Publishing; 2020 Jan-.; 2020. Available from: `https://www.ncbi.nlm.nih.gov/books/NBK553183/`.

27. Johnson PC. Brief Review Autoregulation of Blood Flow. Circulation Research. 1986; p. 483–495.

28. Ursino M, Lodi CA. Interaction among autoregulation, CO2 reactivity, and intracranial pressure: A mathematical model. American Journal of Physiology - Heart and Circulatory Physiology. 1998;doi:10.1152/ajpheart.1998.274.5.h1715.

29. Loutzenhiser R, Bidani A, Chilton L. Renal myogenic response: Kinetic attributes and physiological role. Circulation Research. 2002;90(12):1316–1324. doi:10.1161/01.RES.0000024262.11534.18.

30. Ehmke H. The mechanotransduction of blood pressure. Science. 2018;362(6413):398–399. doi:10.1126/science.aav3495.

31. Kansal N, Clair DG, Jaye DA, Scheiner A. Carotid baroreceptor stimulation blood pressure response mapped in patients undergoing carotid endarterectomy (C-Map study). Autonomic Neuroscience: Basic and Clinical. 2016;201:60–67. doi:10.1016/j.autneu.2016.07.010.

32. Rienzo MD, Parati G, Radaelli A, Castiglioni P. Baroreflex contribution to blood pressure and heart rate oscillations: time scales, time-variant characteristics and nonlinearities. Philosophical Transactions of the Royal Society A: Mathematical, Physical and Engineering Sciences. 2009;367(1892):1301–1318. doi:10.1098/rsta.2008.0274.

33. Wehrwein EA, Joyner MJ. Regulation of blood pressure by the arterial baroreflex and autonomic nervous system. vol. 117. 1st ed. Elsevier B.V.; 2013. Available from: `http://dx.doi.org/10.1016/B978-0-444-53491-0.00008-0`.

34. Wieling W, Krediet CTP, Solari D, De Lange FJ, Van Dijk N, Thijs RD, et al. At the heart of the arterial baroreflex: A physiological basis for a new classification of carotid sinus hypersensitivity. Journal of Internal Medicine. 2013;273(4):345–358. doi:10.1111/joim.12042.

35. Marina N, Christie IN, Korsak A, Doronin M, Brazhe A, Hosford PS, et al. Astrocytes monitor cerebral perfusion and control systemic circulation to maintain brain blood flow. Nature Communications. 2020;11(1):1–9. doi:10.1038/s41467-019-13956-y.

36. Blanco PJ, Trenhago PR, Fernandes LG, Feijóo RA. On the integration of the baroreflex control mechanism in a heterogeneous model of the cardiovascular system. International Journal for Numerical Methods in Biomedical Engineering. 2012;doi:10.1002/cnm.1474.

37. Lau KD, Figueroa CA. Simulation of short-term pressure regulation during the tilt test in a coupled 3D–0D closed-loop model of the circulation. Biomechanics and Modeling in Mechanobiology. 2015;14(4):915–929. doi:10.1007/s10237-014-0645-x.

38. Olufsen MS, Tran HT, Ottesen JT, Lipsitz LA, Novak V, Benim R, et al. Modeling baroreflex regulation of heart rate during orthostatic stress. American Journal of Physiology - Regulatory Integrative and Comparative Physiology. 2006;291(5). doi:10.1152/ajpregu.00205.2006.

39. Ursino M. Interaction between carotid baroregulation and the pulsating heart: A mathematical model. American Journal of Physiology - Heart and Circulatory Physiology. 1998;275(5 44-5):1733–1747. doi:10.1152/ajpheart.1998.275.5.h1733.

40. Blanco P. Rationale for using the velocity–time integral and the minute distance for assessing the stroke volume and cardiac output in point-of-care settings. Ultrasound Journal. 2020;12(1). doi:10.1186/s13089-020-00170-x.

41. Sato K, Fisher JP, Seifert T, Overgaard M, Secher NH, Ogoh S. Blood flow in internal carotid and vertebral arteries during orthostatic stress. Experimental Physiology. 2012;97(12):1272–1280. doi:10.1113/expphysiol.2012.064774.

42. Boysen NC, Dragon DN, Talman WT. Parasympathetic tonic dilatory influences on cerebral vessels. Autonomic Neuroscience: Basic and Clinical. 2009;doi:10.1016/j.autneu.2009.01.009.

43. Talman WT, Corr J, Nitschke Dragon D, Wang DQ. Parasympathetic stimulation elicits cerebral vasodilatation in rat. Autonomic Neuroscience: Basic and Clinical. 2007;doi:10.1016/j.autneu.2006.12.002.

44. Chatterjee K, Carman-Esparza CM, Munson JM. Methods to measure, model and manipulate fluid flow in brain. Journal of Neuroscience Methods. 2020;333(December 2019):108541. doi:10.1016/j.jneumeth.2019.108541.

45. Blanco PJ, Müller LO, Watanabe SM, Feijóo RA. On the anatomical definition of arterial networks in blood flow simulations: comparison of detailed and simplified models. Biomechanics and Modeling in Mechanobiology. 2020;19(5):1663–1678. doi:10.1007/s10237-020-01298-4.

46. Ursino M. A mathematical study of human intracranial hydrodynamics part 1-The cerebrospinal fluid pulse pressure. Annals of Biomedical Engineering. 1988;16(4):379–401. doi:10.1007/BF02364625.

47. Ursino M. A mathematical study of human intracranial hydrodynamics part 2-Simulation of clinical tests. Annals of Biomedical Engineering. 1988;doi:10.1007/BF02364626.

48. Ursino M, Lodi CA. A simple mathematical model of the interaction between intracranial pressure and cerebral hemodynamics. Journal of Applied Physiology. 1997;82(4):1256–1269. doi:10.1152/jappl.1997.82.4.1256.

49. Lampe R, Botkin N, Turova V, Blumenstein T, Alves-Pinto A. Mathematical modelling of cerebral blood circulation and cerebral autoregulation: Towards preventing intracranial hemorrhages in preterm newborns. Computational and Mathematical Methods in Medicine. 2014;doi:10.1155/2014/965275.

50. Piechnik SK, Chiarelli PA, Jezzard P. Modelling vascular reactivity to investigate the basis of the relationship between cerebral blood volume and flow under CO2 manipulation. NeuroImage. 2008;doi:10.1016/j.neuroimage.2007.08.022.

51. Panerai RB, Chacon M, Pereira R, Evans DH. Neural network modelling of dynamic cerebral autoregulation: Assessment and comparison with established methods. Medical Engineering and Physics. 2004;26(1):43–52. doi:10.1016/j.medengphy.2003.08.001.

52. Payne S. Cerebral Autoregulation Control of Blood Flow in the Brain. Springer Nature - SpringerBriefs in Bioengineering; 2016.

53. Ottesen JT, Olufsen MS. Functionality of the baroreceptor nerves in heart rate regulation. Computer Methods and Programs in Biomedicine. 2011;doi:10.1016/j.cmpb.2010.10.012.

54. DeBoer RW, Karemaker JM, Strackee J. Hemodynamic fluctuations and baroreflex sensitivity in humans: A beat-to-beat model. American Journal of Physiology - Heart and Circulatory Physiology. 1987;253(3). doi:10.1152/ajpheart.1987.253.3.h680.

55. Lu K, Clark JW, Ghorbel FH, Robertson CS, Ware DL, Zwischenberger JB, et al. Cerebral Autoregulation and Gas Exchange Studied Using A Human Cardiopulmonary Model. Annual International Conference of the IEEE Engineering in Medicine and Biology - Proceedings. 2003;1:395–397. doi:10.1109/iembs.2003.1279683.

56. Piechnik SK, Czosnyka M, Harris NG, Minhas PS, Pickard JD. A model of the cerebral and cerebrospinal fluid circulations to examine asymmetry in cerebrovascular reactivity. Journal of Cerebral Blood Flow and Metabolism. 2001;21(2):182–192. doi:10.1097/00004647-200102000-00010.

57. Ursino M, Di Giammarco P. A mathematical model of the relationship between cerebral blood volume and intracranial pressure changes: The generation of plateau waves. Annals of Biomedical Engineering. 1991;doi:10.1007/BF02368459.

58. Ursino M, Giannessi M, Frapparelli M, Magosso E. Effect of cushing response on systemic arterial pressure. IEEE Engineering in Medicine and Biology Magazine. 2009;28(6):63–71. doi:10.1109/MEMB.2009.934622.

59. Olufsen MS, Ottesen JT, Tran HT, Ellwein LM, Lewis a, Novak V. From Sitting To Standing : Model Development and Validation. North. 2007;99(4):1523–1537.

60. Carlson BE, Arciero JC, Secomb TW. Theoretical model of blood flow autoregulation: Roles of myogenic, shear-dependent, and metabolic responses. American Journal of Physiology - Heart and Circulatory Physiology. 2008;295(4):1572–1579. doi:10.1152/ajpheart.00262.2008.

61. Müller LO, Zhang Q, Contarino C, Celant M, Agarwal N, Linninger AA, et al. Multi-compartment mathematical model for cerebrospinal fluid mechanics coupled to the systemic circulation: application to transverse sinus stenosis. Veins and Lymphatics. 2019;8(2):8433. doi:10.4081/vl.2019.8433.

62. Sweetman B, Xenos M, Zitella L, Linninger AA. Three-dimensional computational prediction of cerebrospinal fluid flow in the human brain. Computers in Biology and Medicine. 2011;doi:10.1016/j.compbiomed.2010.12.001.

63. Heldt T, Shim EB, Kamm RD, Mark RG, Massachusetts. Computational modeling of cardiovascular response to orthostatic stress. Journal of Applied Physiology. 2002;92(3):1239–1254. doi:10.1152/japplphysiol.00241.2001.

64. Diaz-Artiles A, Heldt T, Young LR. Computational model of cardiovascular response to centrifugation and lower body cycling exercise. Journal of Applied Physiology. 2019;127(5):1453–1468. doi:10.1152/japplphysiol.00314.2019.

65. Linninger AA, Tsakiris C, Zhu DC, Xenos M, Roycewicz P, Danziger Z, et al. Pulsatile cerebrospinal fluid dynamics in the human brain. IEEE Transactions on Biomedical Engineering. 2005;52(4):557–565. doi:10.1109/TBME.2005.844021.

66. Linninger AA, Xenos M, Zhu DC, Somayaji MBR, Kondapalli S, Penn RD. Cerebrospinal fluid flow in the normal and hydrocephalic human brain. IEEE Transactions on Biomedical Engineering. 2007;54(2):291–302. doi:10.1109/TBME.2006.886853.

67. Penn RD, Lee MC, Linninger AA, Miesel K, Lu SN, Stylos L. Pressure gradients in the brain in an experimental model of hydrocephalus. Journal of Neurosurgery. 2005;102(6):1069–1075. doi:10.3171/jns.2005.102.6.1069.

68. Sweetman B, Linninger AA. Cerebrospinal fluid flow dynamics in the central nervous system. Annals of Biomedical Engineering. 2011;39(1):484–496. doi:10.1007/s10439-010-0141-0.

69. Zagzoule M, Marc-Vergnes JP. A global mathematical model of the cerebral circulation in man. Journal of Biomechanics. 1986;doi:10.1016/0021-9290(86)90118-1.

70. Lehtinen MK, Bjornsson CS, Dymecki SM, Gilbertson RJ, Holtzman DM, Monuki ES. The choroid plexus and cerebrospinal fluid: Emerging roles in development, disease, and therapy. Journal of Neuroscience. 2013;33(45):17553–17559. doi:10.1523/JNEUROSCI.3258-13.2013.

71. Lun MP, Monuki ES, Lehtinen MK. Development and functions of the choroid plexus-cerebrospinal fluid system; 2015.

72. Avolio AP. Multi-branched model of the human arterial system. Medical & Biological Engineering & Computing. 1980;18(6):709–718. doi:10.1007/BF02441895.

73. Choudhry FA, Grantham JT, Rai AT, Hogg JP. Vascular geometry of the extracranial carotid arteries: An analysis of length, diameter, and tortuosity. Journal of NeuroInterventional Surgery. 2016;8(5):536–540. doi:10.1136/neurintsurg-2015-011671.

74. Watanabe MSM. ADAN: Um Modelo Anatomicamente Detalhado da Rede Arterial Humana para Hemodinâmica Computacional [PhD Thesis]. Laboratório Nacional de Computação Científica. Petrópolis, RJ - Brazil; 2013. Available from: `http://hemolab.lncc.br/adan-web/doc/2013_thesis_mario_sansuke_maranhao_watanabe.pdf`.

75. Davy KP, Seals DR. Total blood volume in healthy young and older men. Journal of Applied Physiology. 1994;doi:10.1152/jappl.1994.76.5.2059.

76. Baumbach GL, Heistad DD. Regional, segmental, and temporal heterogeneity of cerebral vascular autoregulation. Annals of Biomedical Engineering. 1985;13(3-4):303–310. doi:10.1007/BF02584248.

77. Payne SJ. Identifying the myogenic and metabolic components of cerebral autoregulation. Medical Engineering and Physics. 2018;58:23–30. doi:10.1016/j.medengphy.2018.04.018.

78. Giller CA, Bowman G, Dyer H, Mootz L, Krippner W. Cerebral arterial diameters during changes in blood pressure and carbon dioxide during craniotomy. Neurosurgery. 1993;doi:10.1227/00006123-199305000-00006.

79. Johnson PC, Intaglietta M. Contributions of pressure and flow sensitivity to autoregulation in mesenteric arterioles. The American journal of physiology. 1976;doi:10.1152/ajplegacy.1976.231.6.1686.

80. Kontos HA, Wei EP, Navari RM. Responses of cerebral arteries and arterioles to acute hypotension and hypertension. American Journal of Physiology - Heart and Circulatory Physiology. 1978;3(4). doi:10.1152/ajpheart.1978.234.4.h371.

81. Aaslid R, Lindegaard KF, Sorteberg W, Nornes H. Cerebral autoregulation dynamics in humans. Stroke. 1989;20(1):45–52. doi:10.1161/01.STR.20.1.45.

82. Bank AJ, Wilson RF, Kubo SH, Holte JE, Dresing TJ, Wang H. Direct effects of smooth muscle relaxation and contraction on in vivo human brachial artery elastic properties. Circulation Research. 1995;doi:10.1161/01.RES.77.5.1008.

83. Heistad DD, Marcus ML, Gross PM. Effects of sympathetic nerves on cerebral vessels in dog, cat, and monkey. American Journal of Physiology - Heart and Circulatory Physiology. 1978;doi:10.1152/ajpheart.1978.235.5.h544.

84. Tiecks FP, Lam AM, Aaslid R, Newell DW. Comparison of static and dynamic cerebral autoregulation measurements. Stroke. 1995;doi:10.1161/01.STR.26.6.1014.

85. Bezanson J, Edelman A, Karpinski S, Shah VB. Julia: A fresh approach to numerical computing. SIAM Review. 2017;59(1):65–98. doi:10.1137/141000671.

86. Talman WT, Perrone MH, Reis DJ. Acute hypertension after the local injection of kainic acid into the nucleus tractus solitarii of rats. Circulation Research. 1981;48(2):292–298. doi:10.1161/01.RES.48.2.292.

87. Dirnagl U, Pulsinelli W. Autoregulation of cerebral blood flow in experimental focal brain ischemia. Journal of Cerebral Blood Flow and Metabolism. 1990;10(3):327–336. doi:10.1038/jcbfm.1990.61.

88. Kvålseth T. On Normalized Mutual Information: Measure Derivations and Properties. Entropy. 2017;19(11):631. doi:10.3390/e19110631.

89. Grassberger P. Finite sample corrections to entropy and dimension estimates. Physics Letters A. 1988;128(6-7):369–373. doi:10.1016/0375-9601(88)90193-4.

90. Hernández CX, Pande VS. MDEntropy: Information-Theoretic Analyses for Molecular Dynamics. 2017;doi:10.21105/joss.00427.

91. Guyton AC, Hall JE. Textbook of Medical Physiology. 11th ed. Elsevier Inc.; 2006.

92. Ian L Gordon, MD, PhD, Edward A Stemmer, MD, and Samuel E Wilson M. Redistribution of blood flow after carotid endarterectomy. Journal of Vascular Surgery. 1995;22(4):349–360.

93. Countee RW, Vijayanathan T. External carotid artery in internal carotid artery occlusion. Angiographic, therapeutic, and prognostic considerations. Stroke. 1979;10(4):450–460. doi:10.1161/01.STR.10.4.450.

94. Evensen KB, Eide PK. Measuring intracranial pressure by invasive, less invasive or non-invasive means: Limitations and avenues for improvement. Fluids and Barriers of the CNS. 2020;17(1):1–33. doi:10.1186/s12987-020-00195-3.

95. Hlatky R, Valadka AB, Robertson CS. Analysis of dynamic autoregulation assessed by the cuff deflation method. Neurocritical Care. 2006;4(2):127–132. doi:10.1385/NCC:4:2:127.

96. Berend E Westerhof, Nico Westerhof. Uniform tube models with single reflection site do not explain aortic wave travel and pressure wave shape. Physiological Measurement. 2018;39(12).

97. Preuss M, Hoffmann KT, Reiss-Zimmermann M, Hirsch W, Merkenschlager A, Meixensberger J, et al. Updated physiology and pathophysiology of CSF circulation - The pulsatile vector theory. Child's Nervous System. 2013;29(10):1811–1825. doi:10.1007/s00381-013-2219-0.

98. Krieger EM. Time course of baroreceptor resetting in acute hypertension. The American journal of physiology. 1970;218(2):486–490. doi:10.1152/ajplegacy.1970.218.2.486.